Supporting information for

Unveiling Field-Induced Single-Ion Magnetism in Pentacoordinate and Heptacoordinate Cobalt(II), Dysprosium(III) and Terbium(III) Complexes with Tridentate Bis(Benzimidazole)Pyridine Ligand

Nikoleta Malinová,[ab] Ján Pavlik,[a] Kamil Kotrle,[c] Ivan Nemec,[c] Tibor Dubaj[d], Barbora Brachňaková,[abf] Mario Ruben[bf] and Ivan Šalitroš[ae*]

a) Department of Inorganic Chemistry, Faculty of Chemical and Food Technology, Slovak University of Technology in Bratislava. Bratislava SK-81237, Slovakia. *e-mail: ivan.salitros@stuba.sk
b) Institute of Nanotechnology (INT), Karlsruhe Institute of Technology (KIT), Hermann-von-Helmholtz-Platz 1, 76344 Eggenstein-Leopoldshafen (Germany).
c) Department of Inorganic Chemistry, Faculty of Science, Palacký University, 17. listopadu 12, 771 46 Olomouc, Czech Republic
d) Central European Institute of Technology, Brno University of Technology, Purkyňova 123, 61200 Brno, Czech Republic.
e) Department of Physical Chemistry, Faculty of Chemical and Food Technology, Slovak University of Technology in Bratislava, Bratislava SK-81237, Slovakia
f) Institute for Quantum Materials and Technologies (IQMT), Karlsruhe Institute of Technology (KIT), Hermann-von-Helmholtz-Platz 1, 76344, Eggenstein-Leopoldshafen, Germany.

Content

S1 Experimental section

S1.1 Materials and Methods

1-bromo-3-methoxypropane p.a., Cs_2CO_3, dimethylformamide p.a., acetonitrile p.a., chloroform p.a., dichloromethane p.a., $CoBr_2 \cdot 6H_2O$, $CoCl_2.H_2O$, $Co(NO_3).6H_2O$, $DyCl_3 \cdot 6H_2O$ and $TbCl_3 \cdot 6H_2O$ were purchased from Sigma-Aldrich or Mikrochem and used as received without any further purification. The starting material 2,6-bis(1*H*-benzimidazol-2-yl)pyridine was prepared according to a previously reported procedure[1]. FT-IR spectra in the interval from 4000 to 400 cm^{-1} of compounds reported herein were measured on a Nicolet 5700 spectrometer (ATR technique). Elemental analysis of carbon, hydrogen, and nitrogen was carried out with an EA CHNS(O) Flash 1112 instrument. The NMR spectra were recorded on a Bruker DPX 500 spectrometer. The UV–VIS spectra were measured in the solid state on a Specord 200 spectrophotometer in the range of 800–200 nm. X-ray powder diffraction (PXRD) patterns of complexes **1**–**3** were recorded on a Philips PW1820 diffractometer (Bragg–Brentano geometry) using Co-Kα radiation (40 kV, 35 mA). PXRD data for complexes **4** and **5** were collected on a STOE Stadi P diffractometer operating in transmission mode with Cu-Kα radiation. Polycrystalline sample was measured in Si zero-background sample holder over the 2θ range of 3°–60° with a step size of 0.02° at the room temperature. Thermogravimetric analysis was carried out using a simultaneous TG/DTA analyzer SII EXSTAR 6300 (Seiko Instruments, Japan). Each sample (~ 5 mg) was heated up in a nitrogen purge at the heating rate of 5 °C/min from 40 °C until a significant mass loss due to decomposition was observed. Photoluminescence measurements were recorded using a Horiba Fluorolog spectrometer with a 920-photomultiplier tube detector. A 400 nm long pass filter was used to reduce higher-order diffraction peaks often present in spectra. The crystalline samples were placed in between two quartz plates with a drop of mineral oil and cooled to 3 K under vacuum. Excitation and emission spectra were collected in the range 250-400 nm and 400-700 nm, respectively. The excitation slits were all kept at 7.0 nm for all samples and the emission slits were kept at 1.0 nm (for ligand ***L*** and compound **4**) or 0.2 nm (compound **5**).

S1.2 Synthesis

The ligand **L** (2,6-bis(3-methoxypropyl-1*H*-benzimidazol-2-yl)pyridine) was synthesized in a single step from 2,6-bis(benzimidazol-2-yl)pyridine and commercially available 1-bromo-3-methoxypropane in dimethylformamide. The reaction yielded ligand **L**, which was subsequently purified using column chromatography. Coordination of ligand **L** with Co(II) salts ($CoX_2 \cdot 6H_2O$, where X = Cl (**1**), Br (**2**), and $Co(NO_3)_2 \cdot 6H_2O$ (**3**)) and with $LnCl_3 \cdot 6H_2O$ (Ln=Dy for **4**, Tb for **5**) in acetonitrile at elevated temperatures resulted in the formation of single crystals of the reported complexes, grown under diffusion of diethyl ether.

*Synthesis of ligand **L** (2,6-bis(3-methoxypropyl-1H-benzimidazol-2-yl)pyridine)*

Ligand **L** was prepared by the reaction of 2,6-bis(1*H*-benzimidazol-2-yl)pyridine with caesium carbonate and 1-bromo-3-methoxypropane. In a round bottom flask, 2,6-bis(1*H*-benzimidazol-2-yl)pyridine (1g, 3.2 mmol, 1eq) was dissolved in dimethylformamide (5 ml). Upon the complete dissolution of the 2,6-bis(1*H*-benzimidazol-2-yl)pyridine, 5 equivalents of caesium carbonate (5.231 g; 3.2 mmol) were introduced, and the mixture was heated under reflux condenser at 80 °C on an oil bath for one hour. Subsequently, 5 equivalents of 1-bromo-3-methoxypropane (1.743 g; 3.2 mmol) were added, and the mixture was heated at 100°C for 2 hours. The reaction mixture was allowed to cool to room temperature, and the solvent was removed through vacuum distillation. The crude reaction mixture was suspended in 50 ml of water and extracted with three portions of dichloromethane (200 ml), which were combined, and solvent was evaporated using a vacuum rotary evaporator. The desired product was isolated in 84 % (1.23 g, 2.7 mmol) yield in form of orange oil.

Ligand **L:** FT-IR (ATR, $\tilde{\nu}_{max}/cm^{-1}$): 3052 (w, C_{ar}-H), 2921, 2822 (m, $\nu_{as}(C_{al}\text{-H})$), 2921, 2808 (m, C_{al}-H), 1584, 1571, 1434 (m, C_{ar}-C_{ar}, C_{ar}-N). UV-VIS (acetonitrile, λ/nm): 290 (π→π*), 325 (n→π*). ^{1}H NMR

(300 MHz, d_6-DMSO, 25 °C, δ/ppm): 8.33 (d, J = 7 Hz, 2 H), 8.23-8.21 (m, 1 H), 7.79-7.77 (m, 2 H), 7.69-7.67 (m, 2 H), 7.37-7.31 (m, 4H), 4.86 (t, 4 H), 3.06 (p, 4H), 2.85 (s, 6 H), 1.93-1.88 (m, 4 H). ^{13}C NMR (75 MHz, d_6-DMSO, 25 °C, δ/ppm): 150.28, 142.73, 138.99, 136.61, 125.72, 123.79, 122.53, 120.98, 111.51, 79.64, 68.88, 58.02, 41.94, 29.95. UV-VIS (acetonitrile, λ/nm): 294 (π→π*), 326 (n→π*).

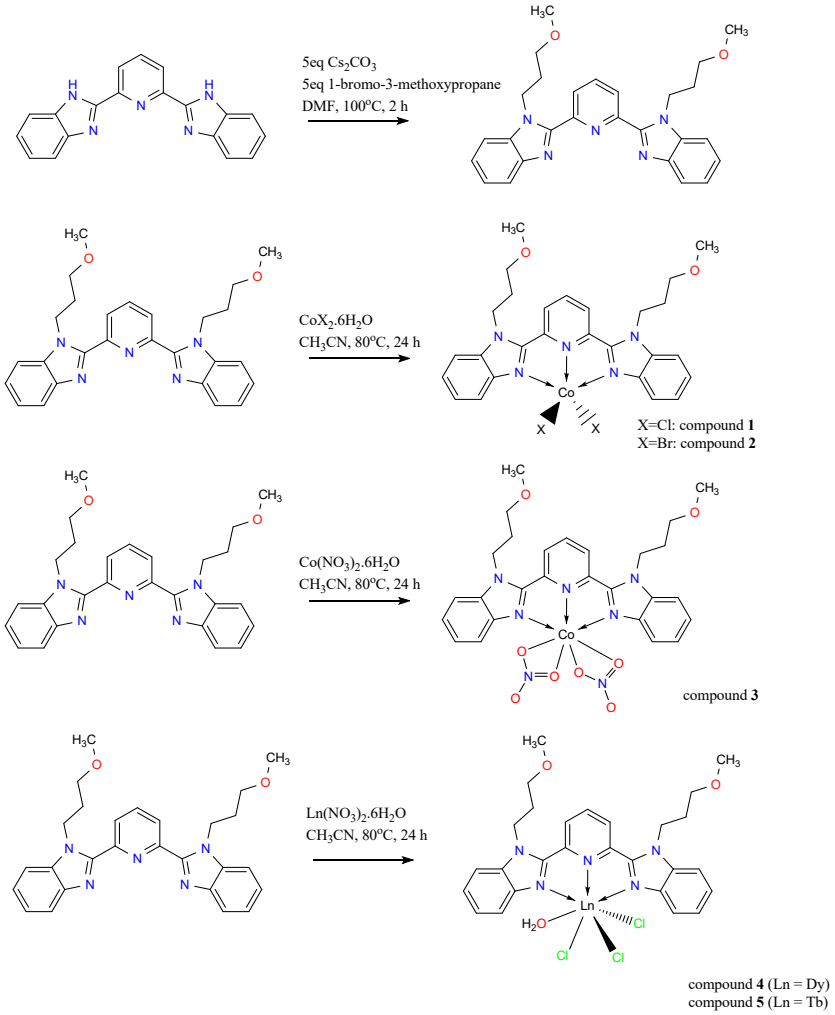

Scheme S1 Synthesis of ligand **L** and complexes **1**-**5**

*Synthesis of complexes **1** [Co(L)Cl$_2$], **2** [Co(L)Br$_2$]*

$CoCl_2 \cdot 6H_2O$ (136 mg, 0.57 mmol, 1.3 eq) or $CoBr_2 \cdot 6H_2O$ (125 mg, 0.38 mmol, 1.3 eq) was dissolved in 10 ml of acetonitrile and added into the acetonitrile solution (30 ml) of ligand **L** (200 mg, 0.44 mmol, 1eq). Upon the addition of Co(II) salt, the colorless solution turned immediately to green without formation of precipitate. The reaction mixture was refluxed for 24 hours and filtered to remove any possible solid impurities. The resulting mother liquor was transferred into smaller test tubes and introduced into a larger bottle partially filled with diethyl ether and stored in the refrigerator. Green crystals **1** or **2** were obtained by diffusion of diethyl ether vapors after several days and collected by filtration. Single-crystal and powder diffraction analyses confirmed that the products are mononuclear Co(II) complexes, whose molecular structure is described by formulas [Co(L)Cl_2] and [Co(L)Br_2].

Complex **1** [Co(L)Cl_2]: Yield 60 % (0.077g, 2.1 mmol). Elemental analysis for $C_{27}H_{29}Cl_2CoN_5O_2$ (585.39 g/mol): calculated (experimental) values C = 55.40 % (54.66 %), N = 11.96 % (11.66 %), H = 4.99 % (4.73%), FT-IR (ATR, $\tilde{\nu}_{max}$/cm^{-1}): 3108 (w, C_{ar}-H), 2981 (w, C_{al}-H), 2928, 2833 (m, C_{al}-H), 2888, 2822 (m, C_{al}-H), 1598, 1566, 1428 (m, C_{ar}-C_{ar}, C_{ar}-N). UV-VIS (acetonitrile, λ/nm): 297, 308 (π→π*), 345 (n→π*); (nujol, λ/nm): 518, 566, 626 (MLCT and/or *d*-*d*).

Complex **2** [Co(L)(Br_2)]: Yield 38 % (0.056 g, 2.1 mmol). Elemental analysis for $C_{27}H_{29}Br_2CoN_5O_2$ (674.29 g/mol): calculated (experimental) values C = 48.09 % (47.32 %), N = 10.39 % (9.47 %), H = 4.33 % (4.07%), FT-IR (ATR, $\tilde{\nu}_{max}$/cm^{-1}): 3109 (w, C_{ar}-H), 2978 (w, C_{al}-H), 2927, 2887 (m, C_{al}-H), 2924, 2805 (m, C_{al}-H), 1598, 1576, 1429 (m, C_{ar}-C_{ar}, C_{ar}-N). UV-VIS (acetonitrile, λ/nm): 311 (π→π*), 344 (n→π*); (nujol, λ/nm): 480, 552 (MLCT and/or *d*-*d*).

*Synthesis of complex **3** [Co(L)(κ^2-NO_3)$_2$]*

Ligand **L** (200 mg, 0.44 mmol, 1eq) was dissolved in acetonitrile (40 ml) and $Co(NO_3)_2 \cdot 6H_2O$ (166 mg, 0.57 mmol, 1.3 eq) was added to it. The addition of the Co(II) salt led to a colour change from light pink to orange-yellowish colour, without formation of precipitate. The solution was then refluxed for 24 hours, filtered, and the mother liquor was poured into small test tubes. The test tubes were then placed into a larger container containing diethyl ether, which was tightly closed and stored in the refrigerator. The orange crystals of **3** were obtained by diffusion of diethyl ether vapors and collected by filtration after several days. Single-crystal and powder diffraction analysis confirmed that product of this reaction is mononuclear Co(II) complex of formula [Co(L)(κ^2-NO_3)$_2$].

Complex **3** [Co(κ^2-L)(NO_3)$_2$]: Yield 62 % (0.087 g, 2.1 mmol). Elemental analysis for $C_{27}H_{29}CoN_7O_8$ (638.49 g/mol): calculated (experimental) values C = 50.79 % (49.92 %), N = 15.36 % (15.04 %), H = 4.58 % (4.34%), FT-IR (ATR, $\tilde{\nu}_{max}$/cm^{-1}): 3088 (w, C_{ar}-H), 2931, 2883, 2831 (m, C_{al}-H), 1598, 1571, 1442 (m-s, (C_{ar}- $C_{ar,}$ C_{ar}-N), 1273 (s, C_{al}-O). UV-VIS (acetonitrile, λ/nm): 310 (π→π*), 343 (n→π*), (nujol, λ/nm): 520, 573, 610 (MLCT and/or *d*-*d*).

*Synthesis of complex **4** [Dy(L)Cl_3(H_2O)] complex **5** [Tb(L)Cl_3(H_2O)]*

$DyCl_3 \cdot 6H_2O$ (59 mg, 0.22 mmol, 1 eq) or $TbCl_3 \cdot 6H_2O$ (42 mg, 0.16 mmol, 1 eq) was dissolved in 15 ml of acetonitrile and added into the acetonitrile solution (10 ml) of ligand **L** (200 mg, 0.015 mmol, 3eq). Upon the addition of Ln(III) salt, the colorless solution without formation of precipitate was observed. The reaction mixture was refluxed for 24 hours and filtered to remove any possible solid impurities. The resulting mother liquor was transferred into smaller test tubes and introduced into a larger bottle partially filled with diethyl ether and stored in the refrigerator. White crystals of **4** or **5** were obtained by diffusion of diethyl ether vapors after several days and collected by filtration. Single-crystal and powder diffraction analyses confirmed that the products are mononuclear Ln(III) complexes, whose molecular structure is described by formulas [Dy(L)Cl_3(H_2O)] and [Tb(L)Cl_3(H_2O)].

Complex **4** [Dy(L)Cl_3(H_2O)]: Yield 43 % (0.005 g, 0.0067 mmol). Elemental analysis for $C_{27}H_{30}Cl_3DyN_5O_3$ (741.41 g/mol): calculated (experimental) values C = 42.99 % (43.74 %), N = 9.01 % (9.45 %), H = 3.78 % (4.08 %). FT-IR (ATR, $\tilde{\nu}_{max}$/cm^{-1}): 3330 (m, O-H), 2930-2850 (m, C_{al}-H), 1651 (m, (C=N) / δ(H–O–H)), 1570-1450 (m, C_{ar}-C_{ar}, C_{ar}-N), 1430-1380 (m, $\delta(CH_3)$). UV-VIS (nujol, λ/nm): 362, 317, 242, 226.

Complex **5** [Tb(L)Cl_3(H_2O)]: Yield 63 % (0.007g, 0.0095 mmol). Elemental analysis for $C_{27}H_{30}Cl_3TbN_5O_3$ (738.85 g/mol): calculated (experimental) values C = 43.15 % (43.95 %), N = 9.05 % (9.49 %), H =3.98 % (4.10 %). FT-IR (ATR, $\tilde{\nu}_{max}$/cm^{-1}): 3147 (w, O-H), 2934 (w, C_{al}-H), 1634 (m, (C=N) / δ(H–O–H)), 1575-1450 (m, C_{ar}-C_{ar}, C_{ar}-N), 1437-1375 (m, $\delta(CH_3)$), 1259-1206 (m, C-O-C), 1118-1033 (m, C-N). UV-VIS (nujol, λ/nm): 370, 245, 323, 227.

S1.3 Diffraction experiments

The single-crystal diffraction data for **1** - **3** were collected at 100 K using an XtaLAB Synergy-I diffractometer with a HyPix3000 hybrid pixel array detector and microfocused PhotonJet-I X-ray source (Cu Kα). The single-crystal diffraction data for **4** and **5** were performed using a "STOE" IPDS 2T diffractometer with an image plate detector and Mo-Kα radiation. The crystals were placed in a cold nitrogen stream (180 K) during data collection. The absorption corrections were applied using the program CrysAlisPro 1.171.40.82a.[2] The structure was solved using SHELXT[3] program and refined by the full matrix least-squares procedure with SHELX[4] in OLEX2 (version 1.5).[5] All non-hydrogen atoms were refined anisotropically. All hydrogen atoms were found from the Fourier difference map and refined using the "riding" model.

S1.4 Magnetic measurements

Herein reported magnetic investigation have been carried out on MPMS SQUID 3 (Quantum design Inc., San Diego, CA, USA). The exact amount of sample was mixed with melted eicosane and filled into the gelatine capsule, which has been used as the sample holder. In the case of magnetic experiments at static magnetic field (DC), the temperature-dependency was recorded in the thermal range 1.9 – 300 K at B = 0.1 T using the 1 K/min sweeping rate, and field-dependency was measured at isothermal conditions in the range B = 0 – 7 T. Collected data were corrected for the diamagnetism of eicosane and gelatine capsule as well as for the molecular diamagnetic contribution, which was calculated using the Pascal constants.[6] Magnetic functions were transformed into the χT vs T and M_{mol} vs B dependencies. The experimental details about the magnetic experiments at AC magnetic field are given in the section S5 (*vide infra*).

S1.5 Computational details

Quantum chemistry calculations of all systems were carried out within the program ORCA 6.1.0[7] and analysis of their magnetic properties was performed with the help of the modules SINGLE_ANISO and POLY_ANISO.[8] All calculations were made with RIJCOSX[9] approximation, improved integral precision ("DEFGRID3" ORCA keyword), and strict convergence ("TightSCF" ORCA keyword).

The positions of all atoms were used as obtained from the X-ray analysis in the case of Co(II) systems. The energy of states of Co(II) systems were calculated using the state averaged complete active space self-consistent field method[10] (SA-CAS[7,5]SCF) complemented by strongly-contracted N-electron valence perturbation theory of second-order (NEVPT2).[11] In either case 10 spin quartet states and 40 spin doublet reference states were taken into account. For all atoms in Co(II) systems the Ahlrichs' basis def2-TZVP[12] was used with auxiliary basis sets def2/J[13] and def2-TZVP/C[14]. In order to calculate the magnetic properties the spin-orbit coupling was included.[15] The ZFS parameters were extracted by quasi-degenerate perturbation theory (QDPT),[16] in which an approximation to the Breit-Pauli form of the spin-orbit coupling operator (variant RI−SOMF(1X) in ORCA 6.1.0)[16b] and the effective Hamiltonian theory were utilized.[17] The magnetic exchange coupling in the case of system **3** was calculated at the DFT level of theory using the abovementioned basis def2-TZVP and hybrid exchange-correlation functional B3LYP.[18]

Fitting of the magnetic susceptibility and magnetization of Co(II) complexes was performed with the program PHI 3.1.6[19].

In the case of Ln(III) complexes the initial molecular structures were treated by DFT hydrogen optimization with the BP86 functional.[20] Calculation of atomic charges was realized using DFT calculation with B3LYP functional. All calculations in Ln(III) systems were performed with X2C relativistic correction.[21] As basis, x2c-TZVPall was used for all atoms except lanthanides (x2c-QZVPall) and C and H (x2c-SVPall).[22] Auxiliary basis was automatically generated via AutoAux[23] option. CASSCF active space was set for electrons in lanthanides' *f*-orbitals via AVAS method.[24] The number of roots was set for 7 with MS = 7, 140 roots with MS = 5, 588 roots with MS = 3 and 490 roots with MS = 1 in the case of Tb(III) system, and

21 roots with MS = 6, 224 roots with MS = 4 and 490 roots with MS = 2 for the Dy(III) system. For analysis of the ligand field, ab initio ligand field theory (AILFT)[25] module was used. Avogadro[26], VESTA[27] and Mercury 2023.3.0[28] programs were applied for visualizations.

S2 Spectral characterization of prepared compounds

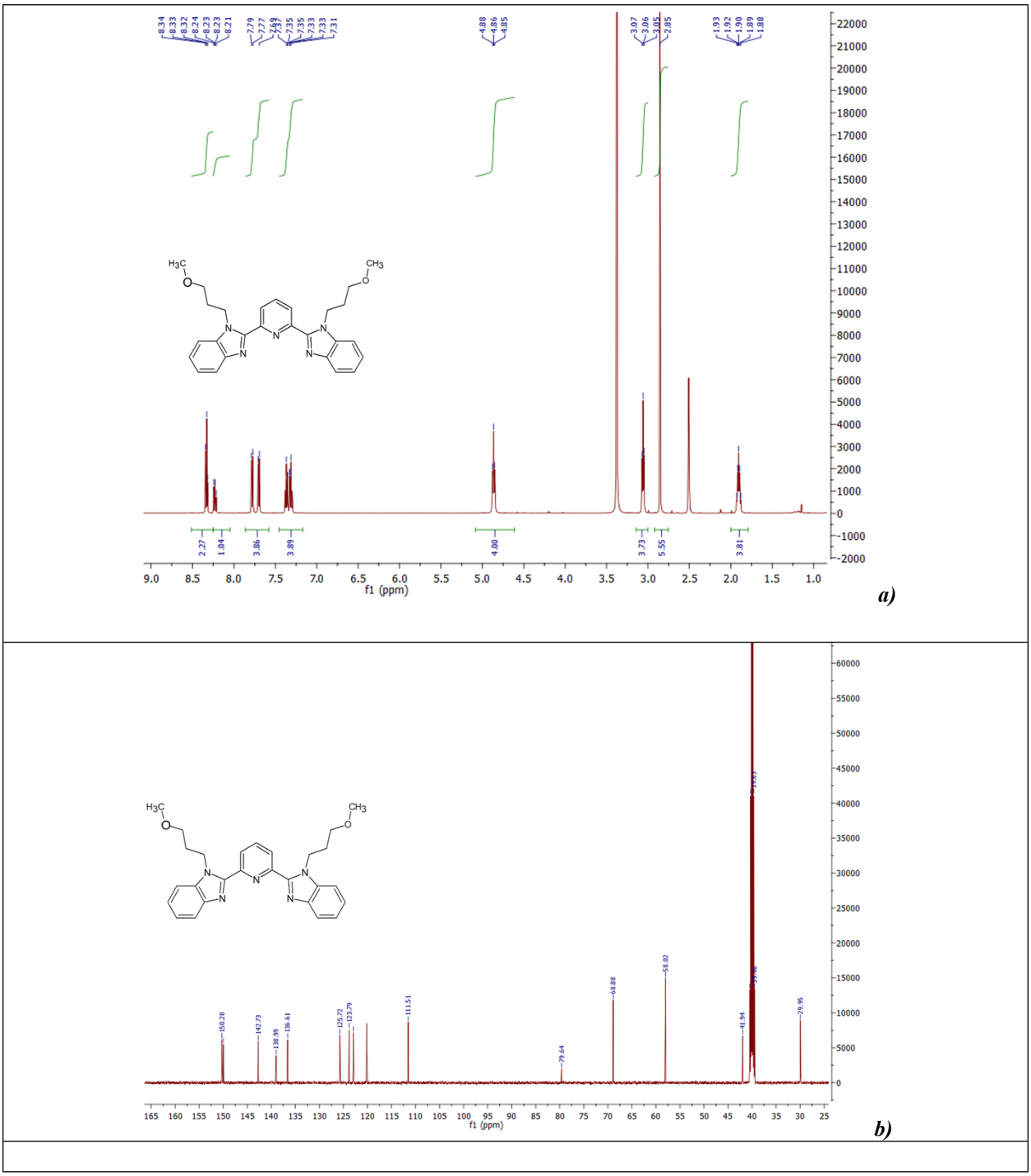

Figure S1 ^{1}H (*a*) and ^{13}C (*b*) NMR spectra for ligand **L**

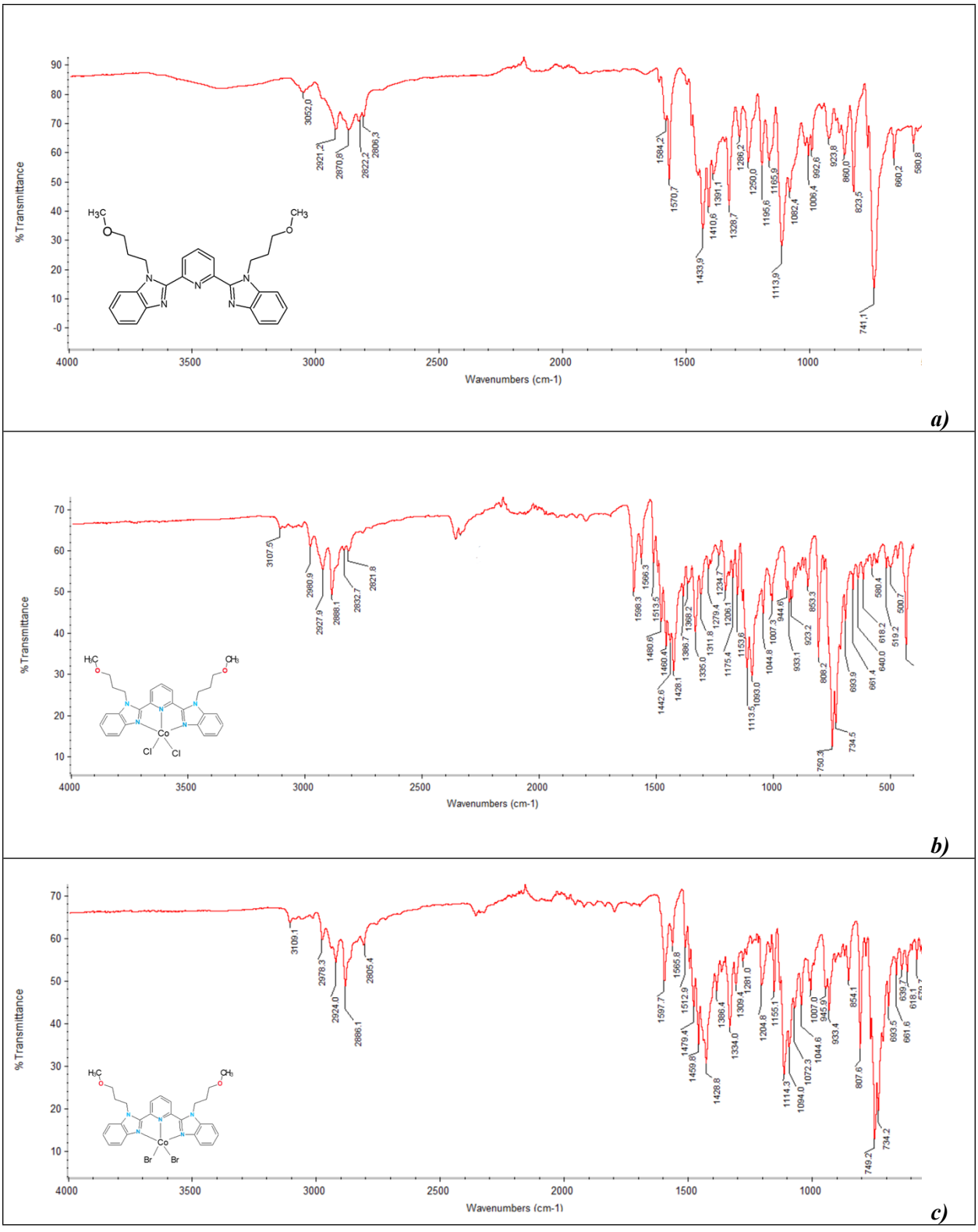
% Transmittance
Wavenumbers (cm-1)
3052,0
2921,2
2870,8
2822,2
2806,3
1584,2
1570,7
1433,9
1410,6
1391,1
1328,7
1286,2
1250,0
1195,6
1165,9
1113,9
1082,4
1006,4
992,6
923,8
860,0
823,5
741,1
660,2
580,8
H3C
CH3
3107,5
2960,9
2927,9
2888,1
2832,7
2821,8
1598,3
1566,3
1513,5
1480,6
1460,4
1442,6
1428,1
1388,7
1368,2
1335,0
1311,8
1279,4
1234,7
1206,1
1176,4
1153,6
1113,5
1093,0
1044,8
1007,3
944,6
933,1
923,2
853,3
808,2
750,3
734,5
693,9
661,4
640,0
618,2
580,4
519,2
500,7
Cl
Cl
Co
3109,1
2978,3
2924,0
2886,1
2805,4
1597,7
1565,8
1512,9
1479,4
1459,8
1428,8
1386,4
1334,0
1309,4
1261,0
1204,8
1155,1
1114,3
1094,0
1072,3
1044,6
1007,0
945,9
933,4
854,1
807,6
749,2
734,2
693,5
661,8
639,7
616,1
Br
Br

a)

b)

c)

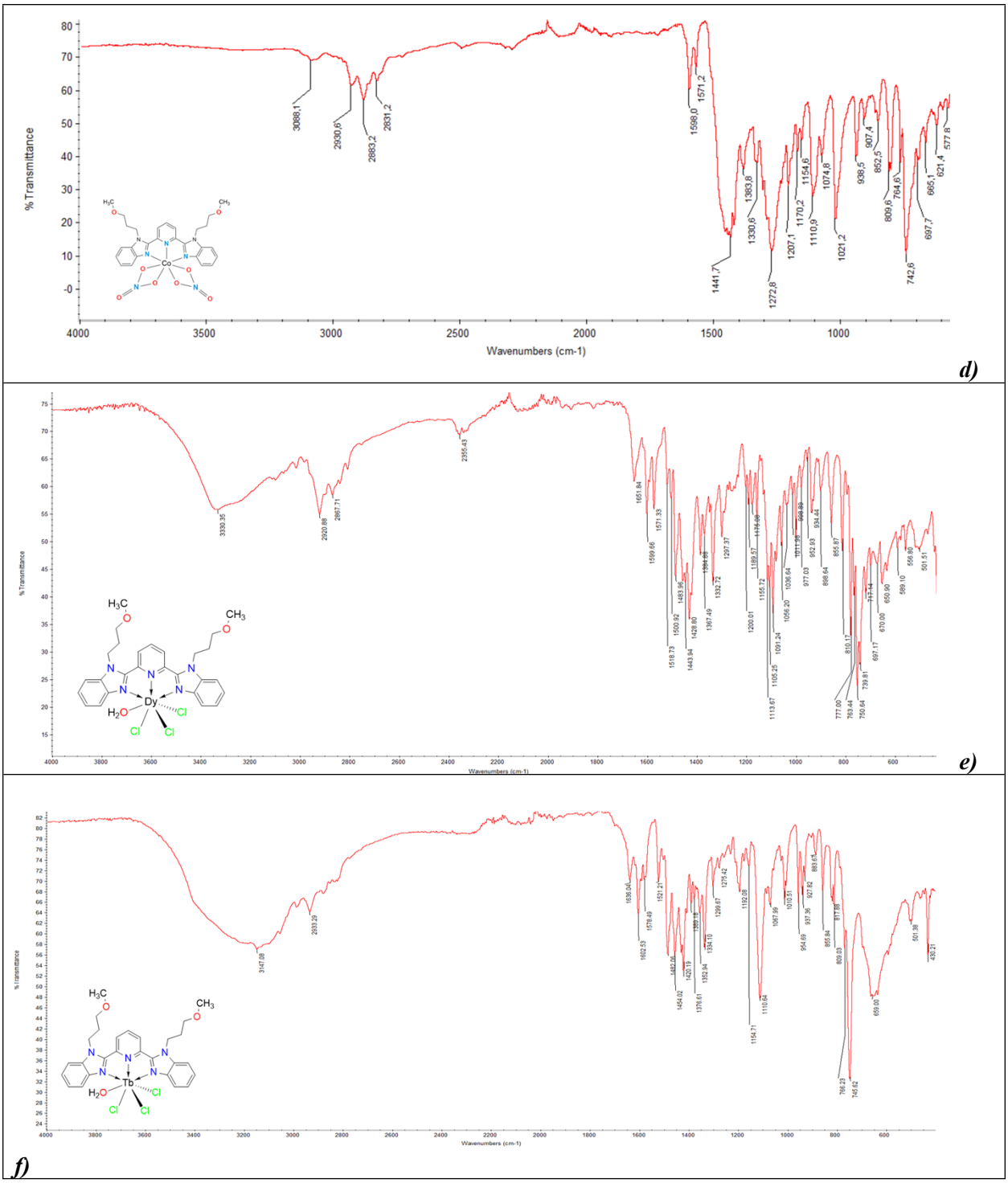

Figure S2 FT-IR spectra of ligand **L** and its complexes **1-5**.

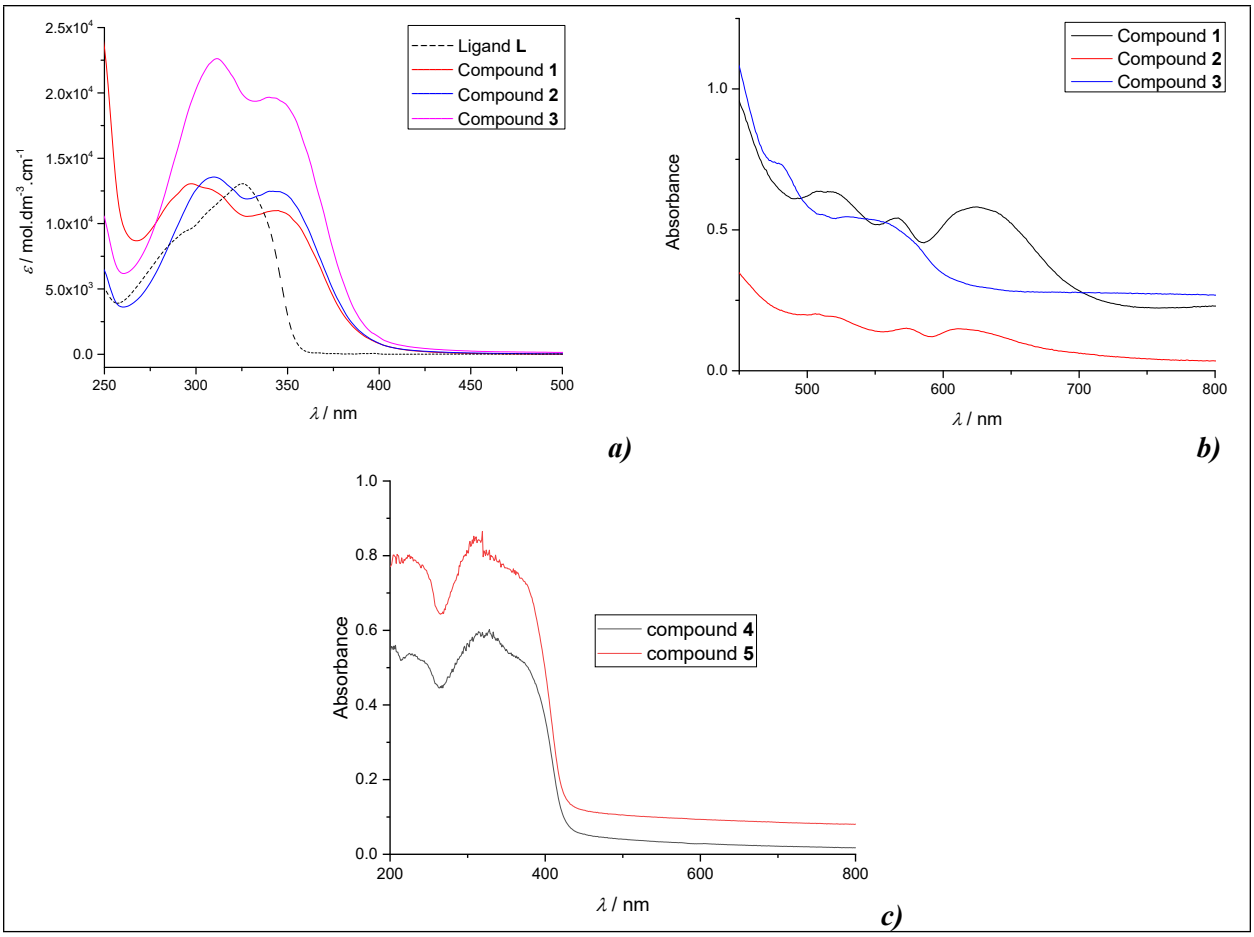

Figure S3 UV-vis spectra of **L**, **1**, **2** and **3** measured in acetonitrile solution (***a***) and in the nujol suspension (***b***) and UV–vis spectra of **4** and **5** recorded in the solid state (in Nujol) (***c***)

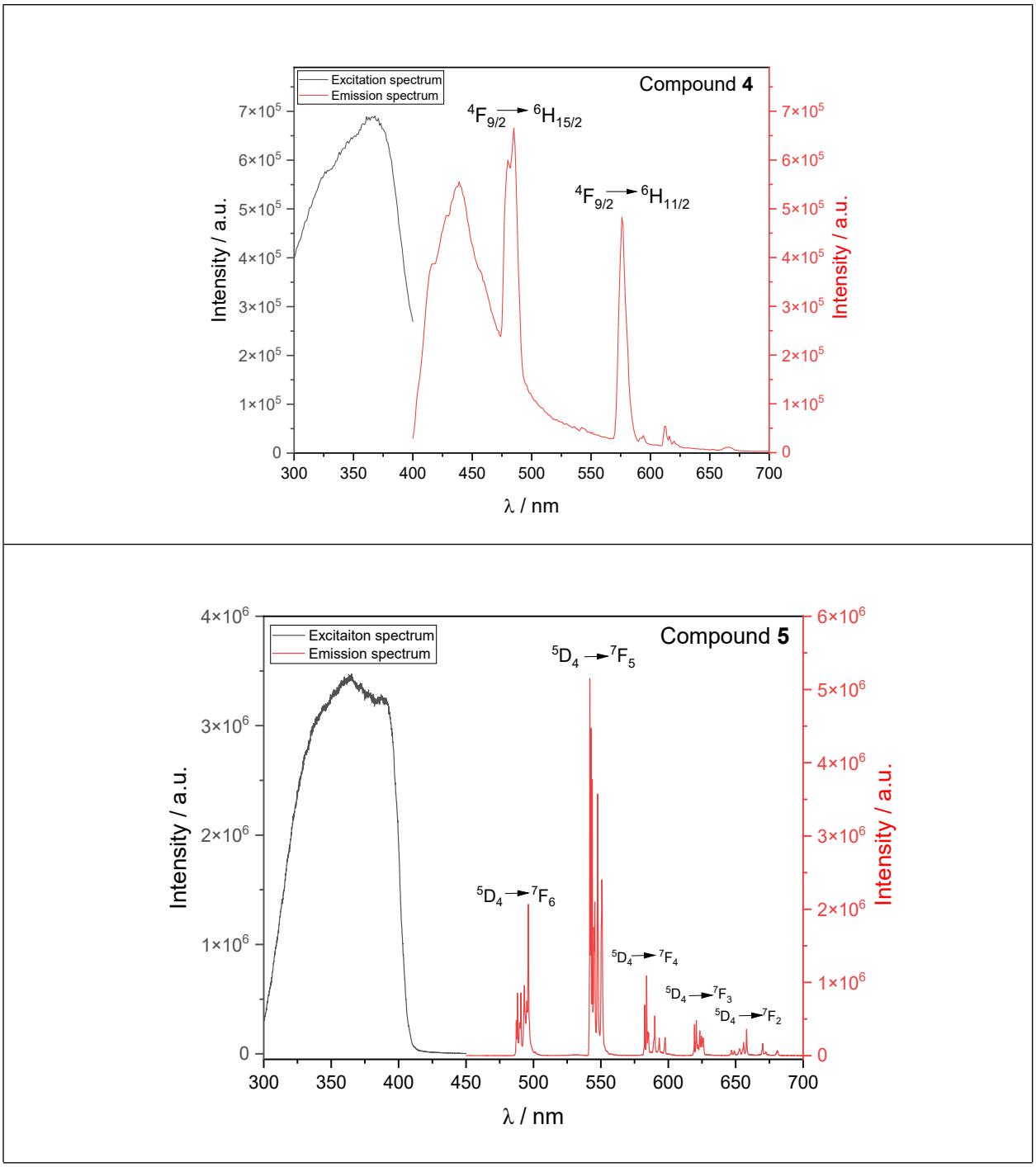

Figure S 4 Steady-state excitation and emission spectra of compound **4** and **5** in the crystalline state at 3 K.

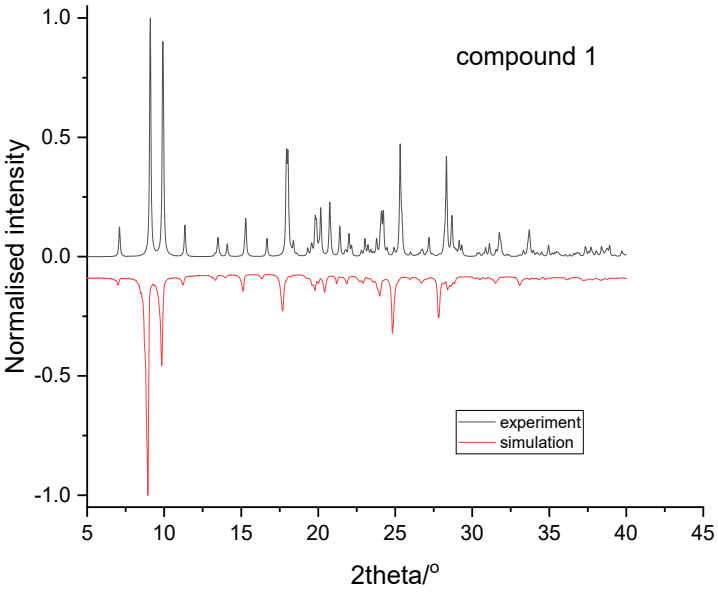
compound 1
Normalised intensity
1.0
0.5
0.0
-0.5
-1.0
5
10
15
20
25
30
35
40
45
2theta/°
experiment
simulation

a)

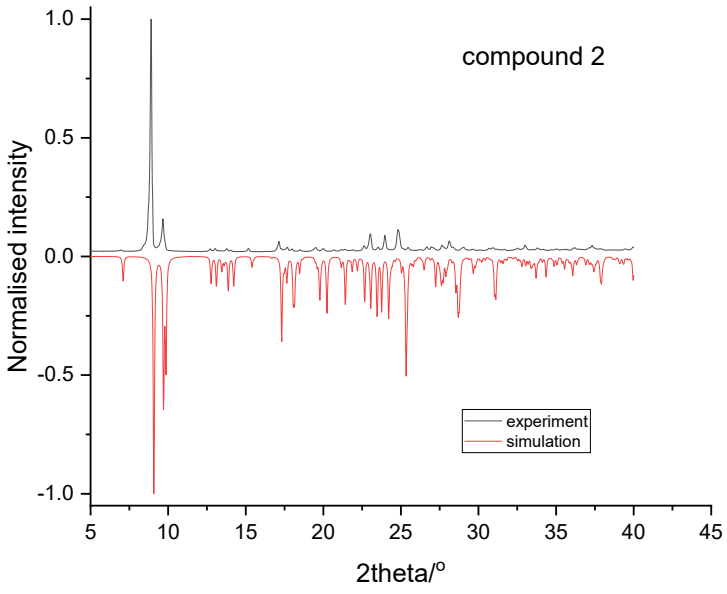
compound 2
Normalised intensity
1.0
0.5
0.0
-0.5
-1.0
5
10
15
20
25
30
35
40
45
2theta/°
experiment
simulation

b)

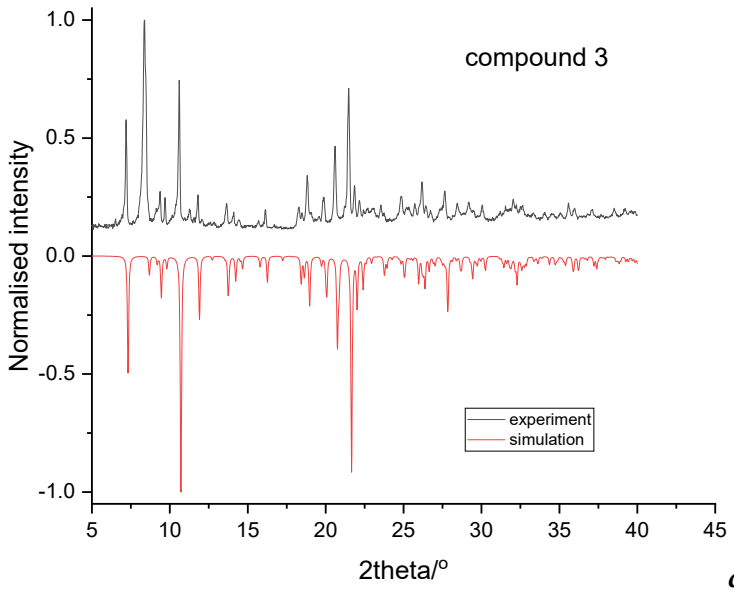
compound 3
Normalised intensity
1.0
0.5
0.0
-0.5
-1.0
5
10
15
20
25
30
35
40
45
2theta/°
experiment
simulation

c)

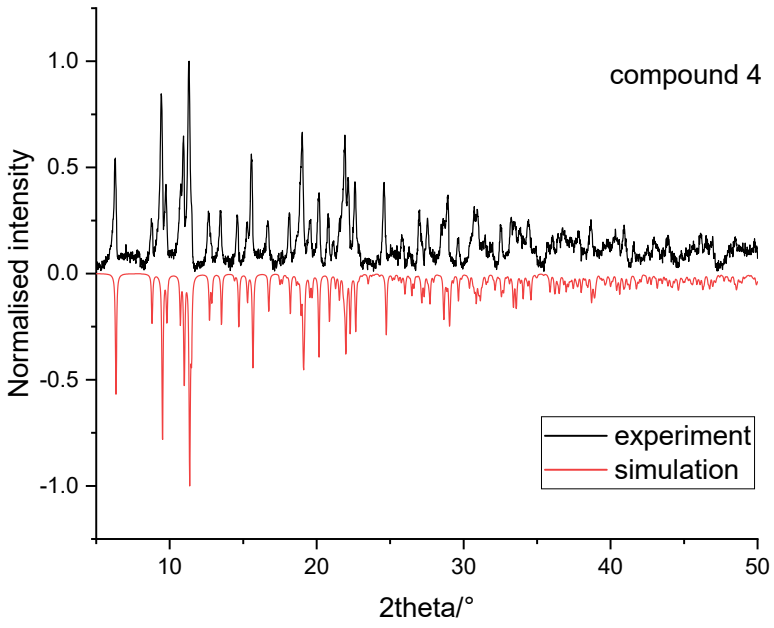
compound 4
Normalised intensity
1.0
0.5
0.0
-0.5
-1.0
10
20
30
40
50
2theta/°
experiment
simulation

d)

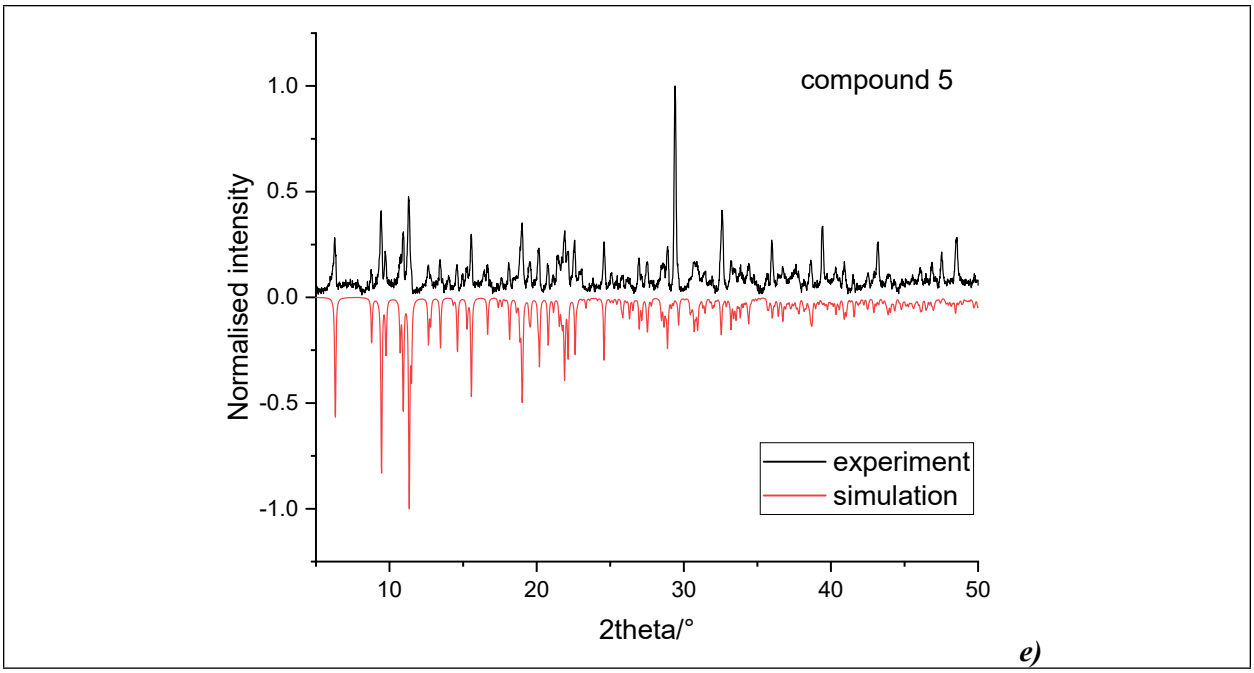

Figure S5 X-ray powder diffraction of **1** (***a***), **2** (***b***), **3** (***c***), **4** (***d***) and **5** (***e***).

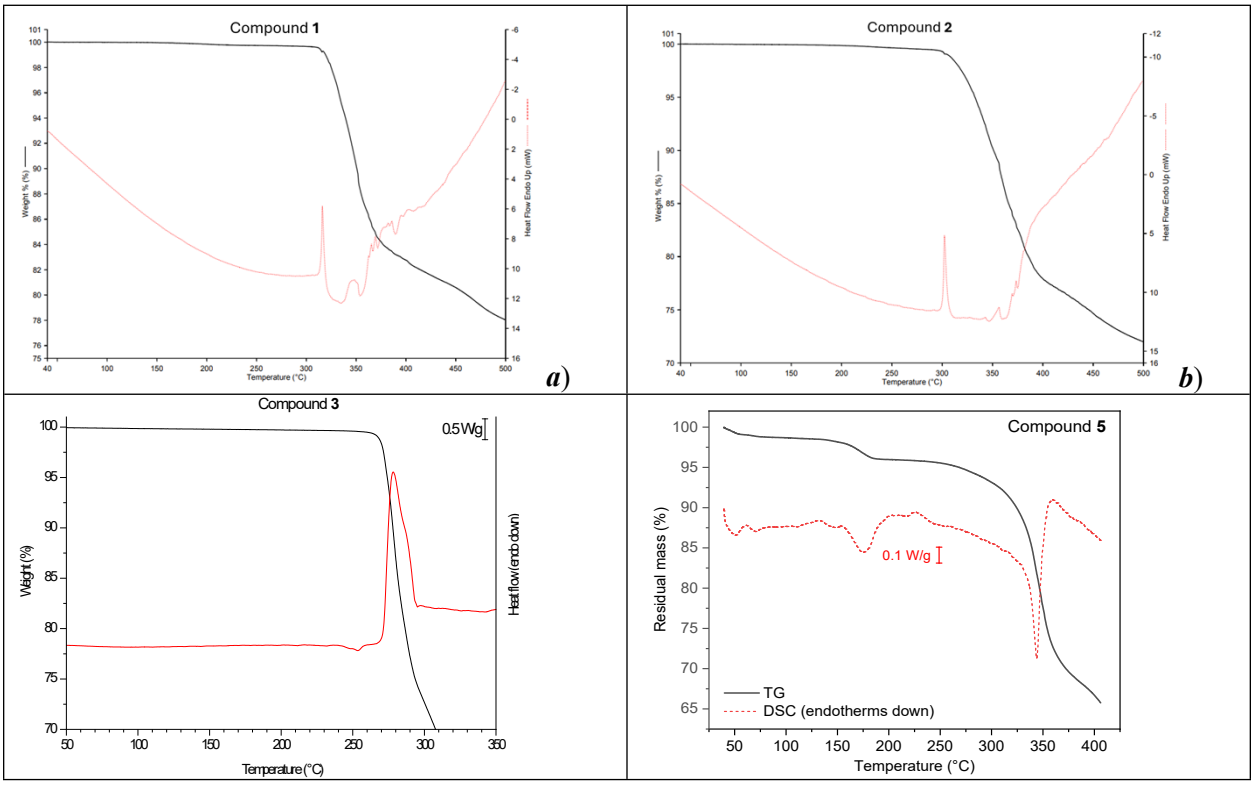

Figure S6 TG/DTA thermal analysis of reported compounds. Observed temperatures of decomposition are 300°C for **1**, 313°C for **2**, 270°C for **3** and 343°C for **5**.

S3 Structural information

Table S1 Structural crystallographic information for reported complexes

	1	**2**	**3**	**4**	**5**
Formula	$C_{27}H_{29}Cl_2CoN_5O_2$	$C_{27}H_{29}Br_2CoN_5O_2$	$C_{27}H_{29}CoN_7O_8$	$C_{27}H_{30}Cl_3DyN_5O_3$	$C_{27}H_{30}Cl_3TbN_5O_3$
M_w / g mol^{-1}	585.38	674.29	638.50	741.41	738.84
T / K	100	100	100	180	293(2)
λ / Å	1.54184	1.54184	1.54184	0.71073	0.71073
Crystal system	triclinic	triclinic	monoclinic	triclinic	triclinic
Space group	$P\bar{1}$	$P\bar{1}$	$P2/c$	$P\bar{1}$	$P\bar{1}$
a / Å	9.6752(2)	9.97860(10)	17.35330(8)	10.0187(6)	10.0638(6)
b / Å	10.7882(2)	10.93360(10)	9.42593(8)	10.3728(5)	10.3747(5)
c / Å	14.0437(3)	13.9927(2)	16.64539(8)	14.5974(8)	14.6603(8)
α / °	108.002(2)	108.8070(10)	90	84.316(4)	84.715(4)
β / °	106.685(2)	103.9280(10)	93.5465(4)	72.513(5)	72.647(5)
γ / °	99.913(2)	103.5930(10)	90	75.452(4)	75.763(5)
Volume / Å^3	1279.47(6)	1318.94(3)	2717.49(2)	1400.04(14)	1415.84(14)
Z; ρ_{calc} / g cm^{-3}	2; 1.519	2; 1.698	4; 1.561	2, 1.759	2, 1.733
μ/mm^{-1}	7.472	8.934	5.518	2.994	2.814
F(000)	606.0	678.0	1324.0	736.0	737.3
Crystal size/mm^3	0.2×0.1×0.07	0.29×0.16×0.13	0.4×0.27×0.21	0.117×0.104×0.036	0.273×0.169×0.082
Final R indices [I> 2σ(I)][a]	R_1 = 0.0273, wR_2 =0.0685	R_1 = 0.0288, wR_2 =0.0775	R_1 = 0.0286, wR_2 = 0.0746	R_1 = 0.0532, wR_2 = 0.1229	R_1 = 0.0387, wR_2 = 0.0967
R indices (all data)[a]	R_1 =0.0279, wR_2 =0.0688	R_1 =0.0295, wR_2 =0.0779	R_1 = 0.0295, wR_2 = 0.0752	R_1 = 0.0642, wR_2 = 0.1295	R_1 = 0.0401, wR_2 = 0.0977
GoF on F^2	1.022	1.027	1.041	1.014	1.019
CCDC no.	2480136	2480137	2480138	2480139	2480140

Table S2 Angles, bond distances and structural parameters of coordination polyhedral calculated for **1** and **2**

1 (100 K)				**2** (100 K)			
angles / °		distances / Å		angles / °		distances / Å	
Cl1-Co1-Cl2	120.959(18)	Co1-Cl1	2.2998(5)	Br1-Co1-Br2	122.520(17)	Co1-Br1	2.4382(5)
N1-Co1-Cl1	95.32(4)	Co1-Cl2	2.3181(5)	N1-Co1-Br1	99.80(5)	Co1-Br2	2.4647(4)
N1-Co1-Cl2	97.51(4)	Co1-N1	2.105(1)	N1-Co1-Br2	96.83(5)	Co1-N1	2.088(2)
N1-Co1-N2	75.19(5)	Co1-N2	2.119(2)	N1-Co1-N2	75.40(7)	Co1-N2	2.109(2)
N1-Co1-N3	147.76(6)	Co1-N3	2.098(1)	N1-Co1-N3	148.52(8)	Co1-N3	2.101(2)
N2-Co1-Cl1	99.35(4)	*d*(Co···{N1,N2, N3,Cl2})	0.5871(7)	N2-Co1-Br1	98.54(5)	*d*(Co···{N1,N2, N3,Br2})	0.6025(11)
N2-Co1-Cl2	139.64(4)			N2-Co1-Br2	138.92(5)		
N3-Co1-Cl1	101.62(4)	SHAPE*		N3-Co1-Br1	96.51(5)	SHAPE*	
N3-Co1-Cl2	96.96(4)	PP-5	33.720	N3-Co1-Br2	96.79(5)	PP-5	33.809
N3-Co1-N2	75.12(5)	vOC-5	4.579	N3-Co1-N2	75.67(7)	vOC-5	5.473
		TBPY-5	4.022			TBPY-5	4.346
		SPY-5	2.221			SPY-5	2.838
		JTBPY-5	8.297			JTBPY-5	9.248
		τ_5	0.31			τ_5	0.27

*PP-5=Pentagon; vOC-5=Vacant octahedron; TBPY-5=Trigonal bipyramid; SPY-5=Spherical square pyramid; JTBPY-5=Johnson trigonal bipyramid J12

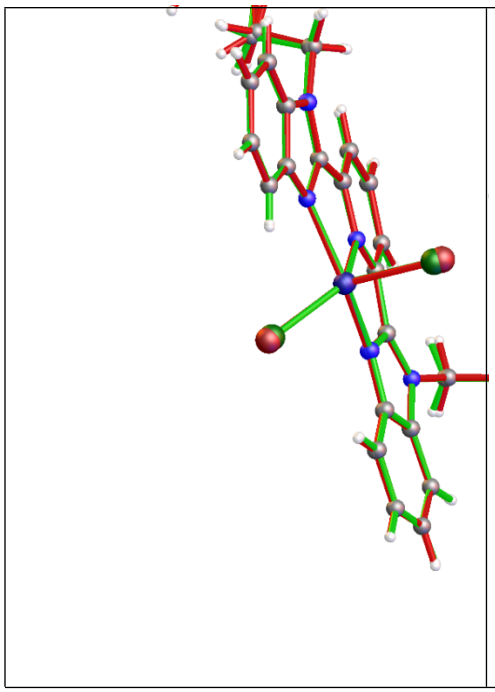

	1/°		**2**/°	**|1-2|**/°
X_{ap}-Co-X_{bas}	120.96(2)	X_{ap}-Co-X_{bas}	122.52(2)	1.56
X_{ap}-Co-N1	92.32(5)	X_{ap}-Co-N3	96.51(4)	4.19
X_{ap}-Co-N2	99.35(4)	X_{ap}-Co-N2	98.54(6)	0.81
X_{ap}-Co-N3	101.62(4)	X_{ap}-Co-N1	99.80(6)	1.82
N1-Co-N2	75.19(6)	N3-Co-N2	75.68(8)	0.49
N2-Co-N3	75.12(6)	N2-Co-N1	75.40(8)	0.28
N3-Co-X_{bas}	96.96(4)	N1-Co-X_{bas}	96.83(6)	0.13
N1-Co-X_{bas}	97.51(5)	N3-Co-X_{bas}	96.79(6)	0.72
N2-Co-X_{bas}	139.64(4)	N2-Co-X_{bas}	138.92(6)	0.72
N1-Co-N3	147.76(6)	N1-Co-N3	148.52(8)	0.76
				δ^{ClBr}= 11.48

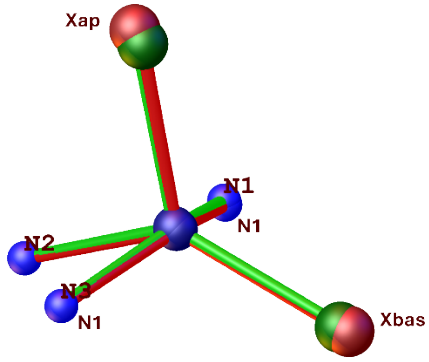

Figure S7 The overlay of molecular structures and coordination polyhedral of **1** (green) and **2** (red). The inserted tables compare 10 angles of the coordination polyhedra, showing the summation of absolute value differences (parameter δ).

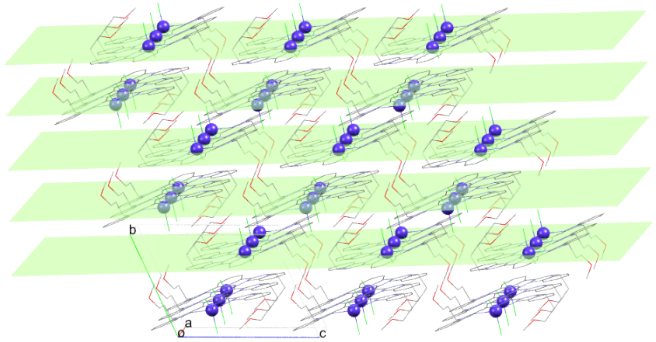

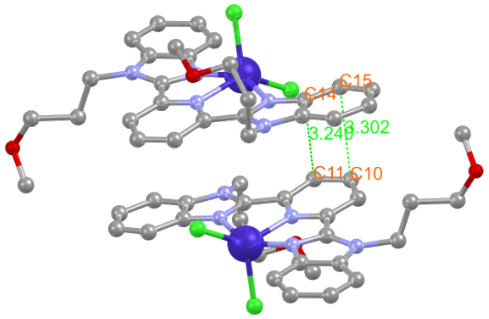

a) compound **1**

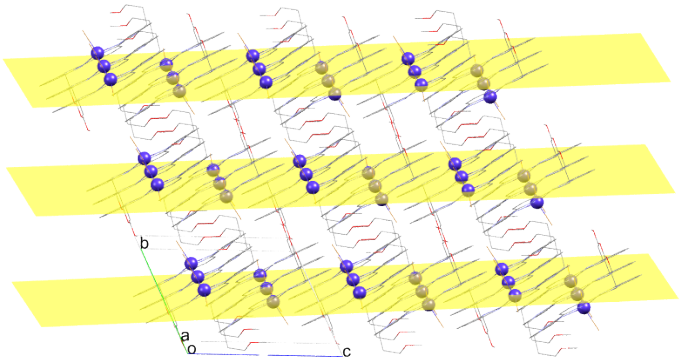

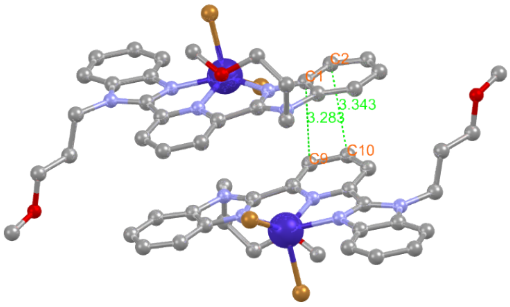

b) compound **2**

Figure S 8 Intermolecular packing and π···π non-covalent contacts for compound **1** (***a***) (C14….C11 = 3.240(3) Å, C15….C10 = 3.302(3) Å) and compound **2** (***b***) (C1….C9 = 3.283(3) Å, C2….C10 = 3.343(4) Å)

Table S3 Angles, bond distances and structural parameters of coordination polyhedral calculated for **3**

angles / °		distances / Å		angles / °		SHAPE* for Co1	
O1-Co1-O1	170.86(6)	Co1-N1	2.1134(12)	O4-Co2-O4	83.38(6)	HP-7	34.043
O2-Co1-O1	131.51(4)	Co1-N2	2.0975(17)	O4-Co2-O5	57.05(4)	HPY-7	19.499
O2-Co1-O1	57.26(4)	Co1-O1	2.3140(11)	O4-Co2-O5	139.73(4)	PBPY-7	4.537
O2-Co1-O2	80.07(6)	Co1-O2	2.1527(11)	O5-Co2-O5	163.13(5)	COC-7	4.455
N1-Co1-O1	86.70(4)	Co2-N5	2.0929(11)	N5-Co2-O4	95.94(4)	**CTPR-7**	**2.704**
N1-Co1-O1	91.10(4)	Co2-N6	2.0794(17)	N5-Co2-O4	103.47(4)	JPBPY-7	7.125
N1-Co1-O2	112.14(5)	Co1-O4	2.1297(11)	N5-Co2-N5	153.96(7)	JETPY-7	19.651
N1-Co1-O2	89.59(4)	Co1-O5	2.3532(11)	N6-Co2-O4	138.31(3)	SHAPE* for Co2	
N1-Co1-N1	152.06(7)			N5-Co2-O5	88.99(4)	HP-7	33.844
N2-Co1-O1	85.43(3)			N6-Co2-O5	81.56(3)	HPY-7	20.077
N2-Co1-O2	139.97(3)			N5-Co2-O5	87.22(4)	**PBPY-7**	**2.801**
N2-Co1-N1	76.03(3)			N6-Co2-N5	76.98(3)	COC-7	6.736
						CTPR-7	4.826
				δ_{eq} (Co2)	60.4(7)	JPBPY-7	5.158
						JETPY-7	20.947

*HP-7=Heptagon; HPY-7=Hexagonal pyramid; PBPY-7=Pentagonal bipyramid; COC-7=Capped octahedron; CTPR-7=Capped trigonal prism; JPBPY-7=Johnson pentagonal bipyramid J13; JETPY-7=Johnson elongated triangular pyramid J7;

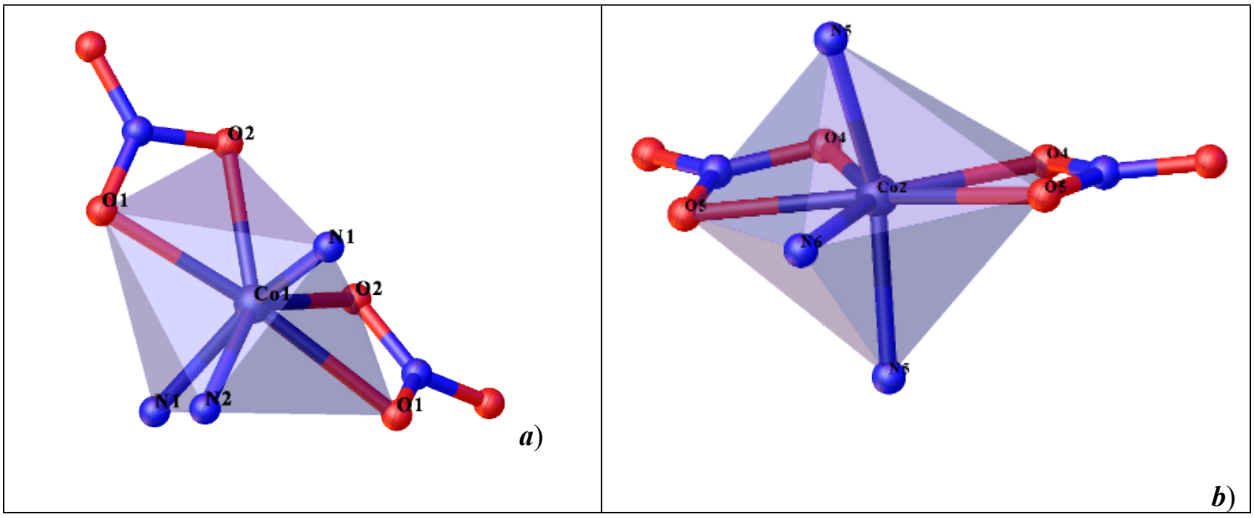

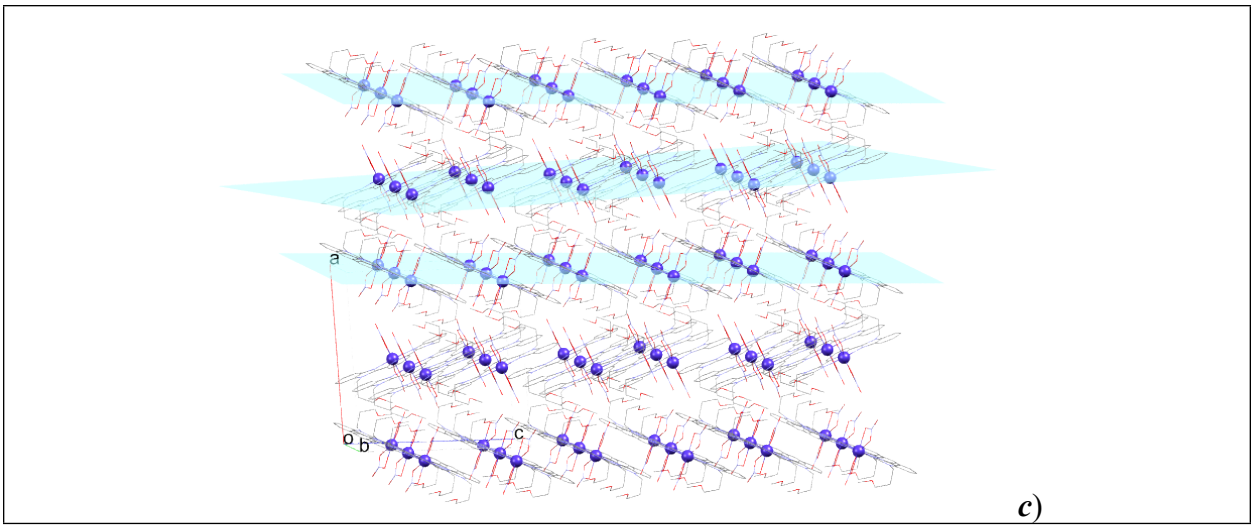

***c*)**

Figure S 9 Capped trigonal prismatic (***a***) and pentagonal bipyramidal (***b***) shapes of coordination polyhedra in crystal structure of **3.** Crystal packing of $[Co(L)(\kappa^2\text{-}NO_3)_2]$ molecules viewed along the *b*-*c* plane of crystal structure **3** (***c*)**

Table S4 Angles, bond distances and structural parameters of coordination polyhedra calculated for **4** and **5**

Compound **4**				Compound **5**			
angles / °		**distances / Å**		**angles / °**		**distances / Å**	
Cl2-Dy-Cl1	95.04(5)	Dy1-Cl1	2.6646(15)	Cl2-Tb1-Cl1	95.42(3)	Tb1-Cl1	2.6769(9)
Cl2-Dy1-Cl3	89.65(6)	Dy1-Cl2	2.6049(15)	Cl2-Tb1-Cl3	89.91(4)	Tb1-Cl2	2.6107(8)
Cl3-Dy1-Cl1	175.29(5)	Dy1-Cl3	2.6128(17)	Cl3-Tb1-Cl1	174.62(3)	Tb1-Cl3	2.6182(9)
O1-Dy1-Cl1	81.28(11)	Dy1-O1	2.418(4)	O1-Tb1-Cl1	81.31(6)	Tb1-O1	2.439(2)
O1-Dy1-Cl2	77.02(10)	Dy1-N2	2.593(5)	O1-Tb1-Cl2	76.76(6)	Tb1-N2	2.603(2)
O1-Dy1-Cl3	100.32(11)	Dy1-N3	2.500(5)	O1-Tb1-Cl3	100.70(6)	Tb1-N3	2.499(2)
O1-Dy1-N2	127.92(14)	Dy1-N1	2.493(5)	O1-Tb1-N2	127.80(8)	Tb1-N1	2.508(2)
O1-Dy1-N3	162.57(15)			O1-Tb1-N3	73.99(8)		
O1-Dy1-N1	74.00(15)	δ_{eq}	58.2(2)	O1-Tb1-N1	162.90(9)	δ_{eq}	51.48(8)
N2-Dy1-Cl1	73.96(12)	**SHAPE***		N2-Tb1-Cl1	74.13(6)	**SHAPE***	
N2-Dy1-Cl2	148.83(11)	HP-7	34.166	N2-Tb1-Cl2	149.55(6)	HP-7	33.998
N2-Dy1-Cl3	101.71(12)	HPY-7	20.605	N2-Tb1-Cl3	100.84(6)	HPY-7	20.530
N3-Dy1-Cl1	90.13(12)	**PBPY-7**	2.346	N3-Tb1-Cl1	94.79(6)	**PBPY-7**	**2.332**
N3-Dy1-Cl2	88.76(12)	COC-7	4.380	N3-Tb1-Cl2	147.08(6)	COC-7	4.435
N3-Dy1-Cl3	89.46(12)	CTPR-7	3.270	N3-Tb1-Cl3	81.06(6)	CTPR-7	3.386
N3-Dy1-N2	62.76(15)	JPBPY-7	6.939	N3-Tb1-N2	63.31(8)	JPBPY-7	6.914
N1-Dy1-Cl1	95.12(12)	JETPY-7	20.440	N3-Tb1-N1	121.79(8)	JETPY-7	20.568
N1-Dy1-Cl2	147.36(13)			N1-Tb1-Cl1	90.21(6)		
N1-Dy1-Cl3	81.14(12)			N1-Tb1-Cl2	89.39(6)		
N1-Dy1-N2	63.74(16)			N1-Tb1-Cl3	89.09(6)		
N1-Dy1-N3	122.14(17)			N1-Tb1-N2	62.69(8)		

*HP-7=Heptagon; HPY-7=Hexagonal pyramid; PBPY-7=Pentagonal bipyramid; COC-7=Capped octahedron; CTPR-7=Capped trigonal prism; JPBPY-7=Johnson pentagonal bipyramid J13; JETPY-7=Johnson elongated triangular pyramid J7;

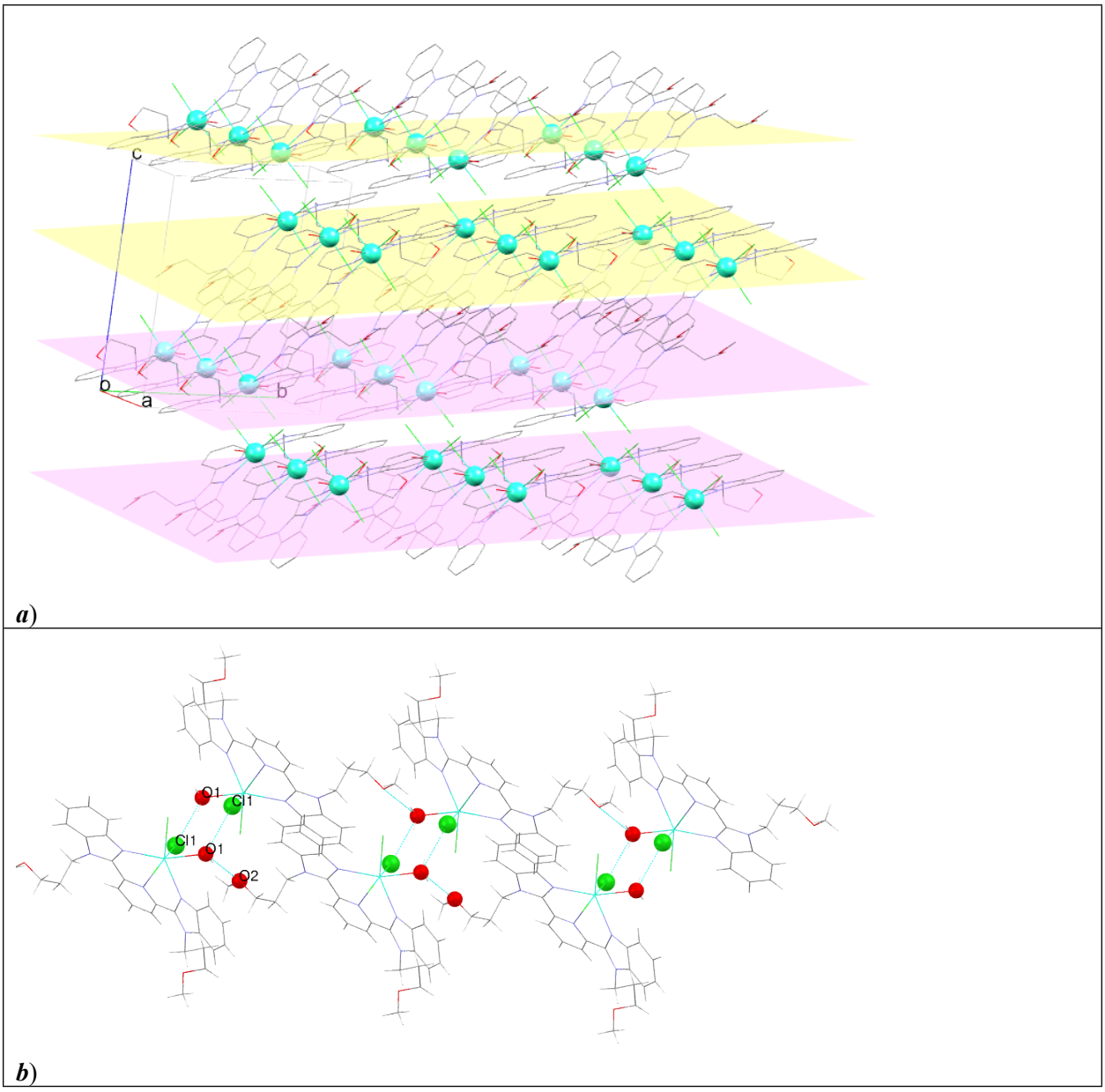

a)

b)

Figure S 10 a) Crystal packing of complexes **4** and **5** viewed along the *a*–*b* plane. Yellow and violet layers represent molecules facing each other through chlorido ligands, with shorter interlayer separations of 6.336(7) Å (**4**) and 6.304(5) Å (**5**). Mutual arrangement of molecules facing each other through tridentate ligand **L** is represented between yellow and violet layers, whit longer separation (7.612(5) Å for **4** and 7.716(6) Å for **5**). ***b***) Hydrogen-bonded networks in **4** (O1···Cl1 = 3.227(5) Å, O1···O2 = 2.790(6) Å) and **5** (O1···Cl1 = 3.237(3) Å, O1···O2 = 2.814(3) Å), formed between molecules within and between the yellow layers.

S4 Computational Study and Static Magnetic Properties

S4.1 Ab-initio calculation and analysis of magnetic measurements

Table S 5 Energy of lowest Kramers' doublets in cm^{-1} for **1**, **2**, **3ctp** and **3pbp** calculated by CAS[7,5]SCF-NEVPT2. Different font colors show the states associated in common spin quartet.

1	2	3 ctp	3pbp
0.0	0.0	0.0	0.0
166.6	224.0	37.8	79.4
538.8	486.0	3217.3	2509.5
762.5	780.0	3475.1	2994.6
2007.3	2231.0	4378.1	3466.7
2090.2	2295.4	4496.4	3868.1

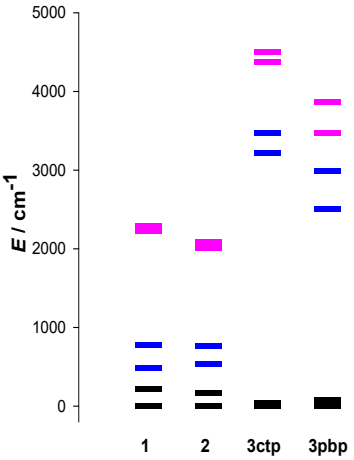

Figure S 11 Energy of lowest Kramers doublets in cm^{-1} for **1**, **2**, **3ctp** and **3pbp** calculated by CAS[7,5]SCF-NEVPT2. Different font colours show the states associated in common spin quartet.

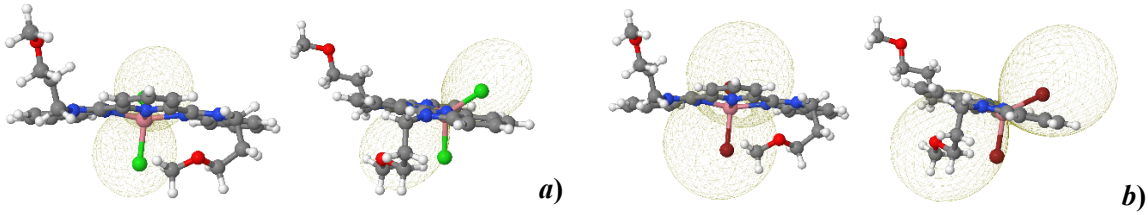

a) ***b)***

Figure S 12 Isosurface plot of local molecular magnetization at magnetic field of 0.1T and temperature of 2.0 K as resulted from the *ab-initio* calculation. Rear and side view of **1** (***a***); rear and side view of **2** (***b***).

Table S 6 Optimum values of Spin Hamiltonian parameters extracted from experimental data.

	1	2
D[cm^{-1}]	57.2	61.0
E/D	--	--
g_x	2.90	2.42
g_y	2.20	2.95
g_z	1.77	2.00
zJ[cm^{-1}]	-0.012	-0.039
χ_{TIP}[$cm^3.K.mol^{-1}$]	0.001	0.001
R	0.0068	0.0001

Table S 7 Orientations of g-tensor axes for KD1 and KD2 and relative orientations of the main axis of magnetization for the systems **1** and **2**.

1	**2**
KD1 MAIN VALUES | MAIN MAGNETIC AXES gX = 1.07743696 | Xm | 0.522249 -0.825009 -0.215908 gY = 1.32528660 | Ym | -0.089580 0.198706 -0.975957 gZ = 8.93692098 | Zm | 0.848075 0.529033 0.029870 **KD2** MAIN VALUES | MAIN MAGNETIC AXES gX = 1.62902602 | Xm | 0.059969 -0.340991 0.938152 gY = 2.71467251 | Ym | 0.555917 -0.769194 -0.315115 gZ = 4.23559317 | Zm | 0.829072 0.540431 0.143435 Relative angle of main axes: 7.3°	**KD1** MAIN VALUES | MAIN MAGNETIC AXES gX = 1.62514650 | Xm | -0.532023 0.810891 -0.243736 gY = 2.70847325 | Ym | 0.097506 -0.227268 -0.968938 gZ = 7.85600910 | Zm | -0.841097 -0.539263 0.041845 **KD2** MAIN VALUES | MAIN MAGNETIC AXES gX = 2.22724449 | Xm | -0.414087 -0.534062 -0.737096 gY = 2.52582526 | Ym | 0.711276 0.315461 -0.628149 gZ = 4.77422375 | Zm | 0.567995 -0.784387 0.249236 Relative angle of main axes: 103°

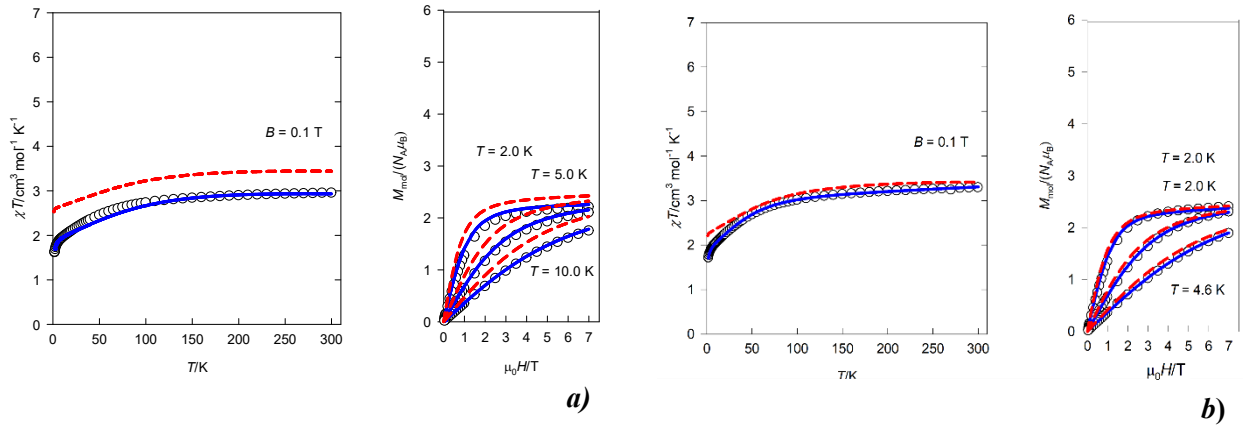

a) ***b)***

Figure S 13 Magnetic functions analyzed by Spin Hamiltonian for compound **1** (***a***) and compound **2** (***b***); left: susceptibility-temperature product with respect to temperature, right: magnetization per center with respect to the magnetic field; empty circles: experiment, blue solid line: optimum fit.

Table S 8 Report of the DFT calculation of magnetic exchange interaction between magnetic centers **3pbp** and **3ctp**, top: excerpt of the calculation input, bottom: excerpt pf calculation output.

```
! uks b3lyp rijcosx def2-tzvp def2/j tightscf veryslowconv uno
! moread

%moinp "/home/jan/Documents/orca503_test/nm/58/double/opt/nm58dblopt.gbw"

%scf
  maxiter  1500
  flipspin 0
  finalms  0.0
end
```

```
-----------------------------------------
BROKEN SYMMETRY MAGNETIC COUPLING ANALYSIS
-----------------------------------------
```

S(High-Spin) = 3.0
<S**2>(High-Spin) = 12.0220
<S**2>(BrokenSym) = 3.0220
E(High-Spin) = -6827.279684 Eh
E(BrokenSym) = -6827.279684 Eh
E(High-Spin)-E(BrokenSym)= 0.0000 eV 0.000 cm**-1 (ANTIFERROMAGNETIC coupling)

| Spin-Hamiltonian Analysis based on H(HDvV)= -2J*SA*SB |

| J(1) = -0.00 cm**-1 (from -(E[HS]-E[BS])/Smax**2) |
| J(2) = -0.00 cm**-1 (from -(E[HS]-E[BS])/(Smax*(Smax+1)) |
| J(3) = -0.00 cm**-1 (from -(E[HS]-E[BS])/(<S**2>HS-<S**2>BS)) |

Table S 9 Optimum values of Spin Hamiltonian parameters extracted from experimental data without inclusion of relative orientation of local *D*-tensors.

	3 ctp	**3pbp**
D[cm^{-1}]	-11.1	34.4
E/D	0.26	0.21
g_x	2.15	2.55
g_y	2.25	2.24
g_z	2.42	2.0*
χ_{TIP}[cm^3.K.mol^{-1}]	0.0019	
R	0.0011	

*The value was not a subject of optimization.

Table S 10 Orientations of *g*-tensor axes for KD1 and KD2 and relative orientations of the main axis of magnetization for the systems **3pbp** and **3ctp**.

3ctp	**3pbp**
KD1 MAIN VALUES | MAIN MAGNETIC AXES gX = 1.20398893 | Xm | -0.316901 -0.000008 0.948459 | gY = 1.55005527 | Ym | -0.948459 -0.000029 -0.316901 | gZ = 6.75818956 | Zm | 0.000031 -1.000000 0.000001 |	**KD1** MAIN VALUES | MAIN MAGNETIC AXES gX = 1.71791322 | Xm | 0.362319 0.000005 0.932054 | gY = 2.87276912 | Ym | -0.932054 0.000001 0.362319 | gZ = 6.32498626 | Zm | 0.000001 -1.000000 0.000005 |
KD2 MAIN VALUES | MAIN MAGNETIC AXES gX = 2.03729415 | Xm | 0.000034 -1.000000 0.000004 | gY = 2.89275760 | Ym | 0.938103 0.000033 0.346356 | gZ = 5.55960286 | Zm | -0.346356 -0.000008 0.938103 |	**KD2** MAIN VALUES | MAIN MAGNETIC AXES gX = 1.43267654 | Xm | 0.000002 -1.000000 0.000004 | gY = 1.65087990 | Ym | 0.935107 0.000000 -0.354365 | gZ = 5.77393519 | Zm | 0.354365 0.000005 0.935107 |
Relative angle of main axes: 90°	Relative angle of main axes: 90°

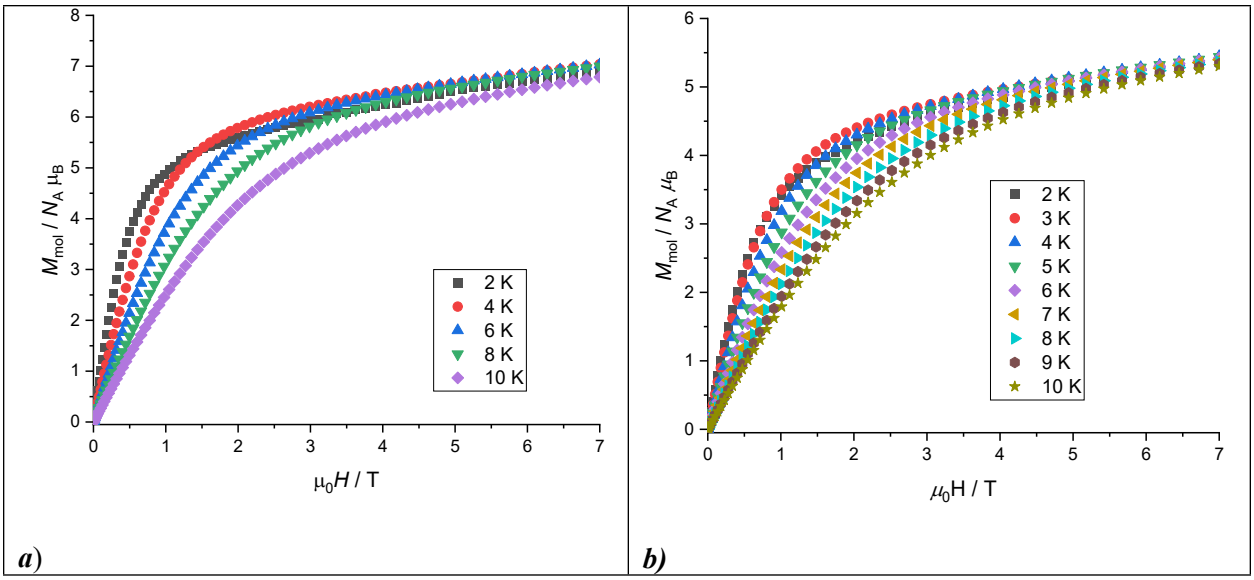

Figure S 14: Field-dependent magnetization data for complexes **4** (left) and **5** (right).

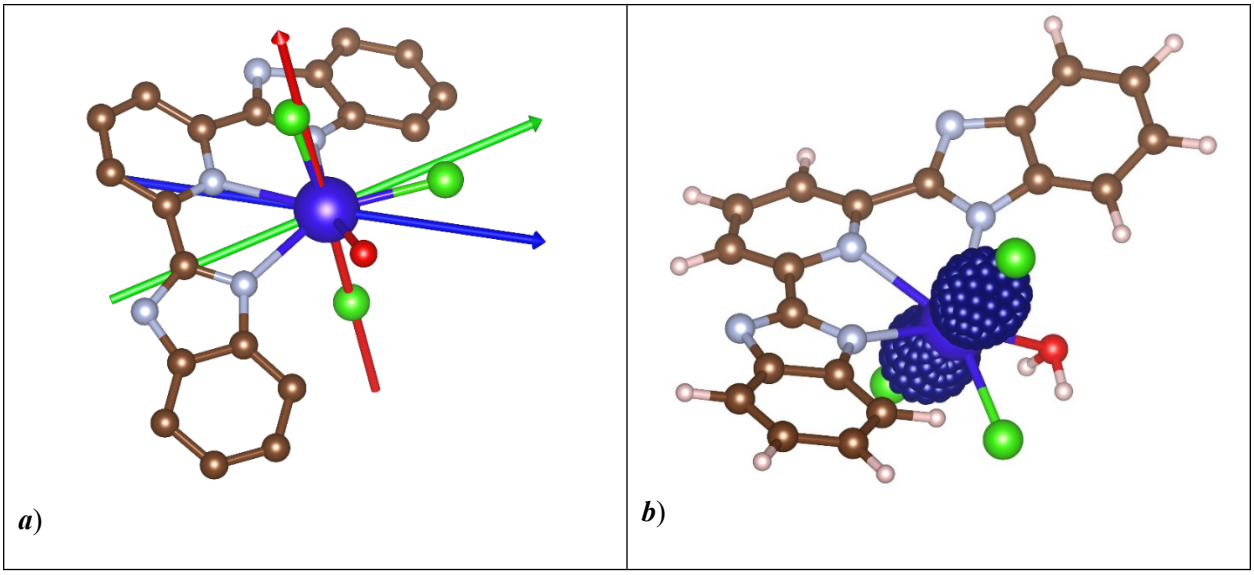

Figure S 15: a) Scheme of direction of main magnetic axis for complex **4** (hydrogen atoms and aliphatic chains have been omitted for clarity), figure shows the direction for ground doublet (red), first excited (green) and second excited (blue) doublets (left). **b**) Projection of magnetization in a spheric grid for **4**.

Table S 11: Energies and *g*-factors of ground state Kramers' doublets of complex **4**

E (cm^{-1})	g_x	g_y	g_z
0.00	0.25	0.66	19.25
86.83	0.99	1.34	17.72
180.27	9.89	7.70	2.61
219.63	0.64	2.50	13.38
291.32	0.02	2.70	12.18
325.98	1.77	4.11	12.26
350.14	1.90	2.28	14.22
408.00	0.39	0.59	17.72

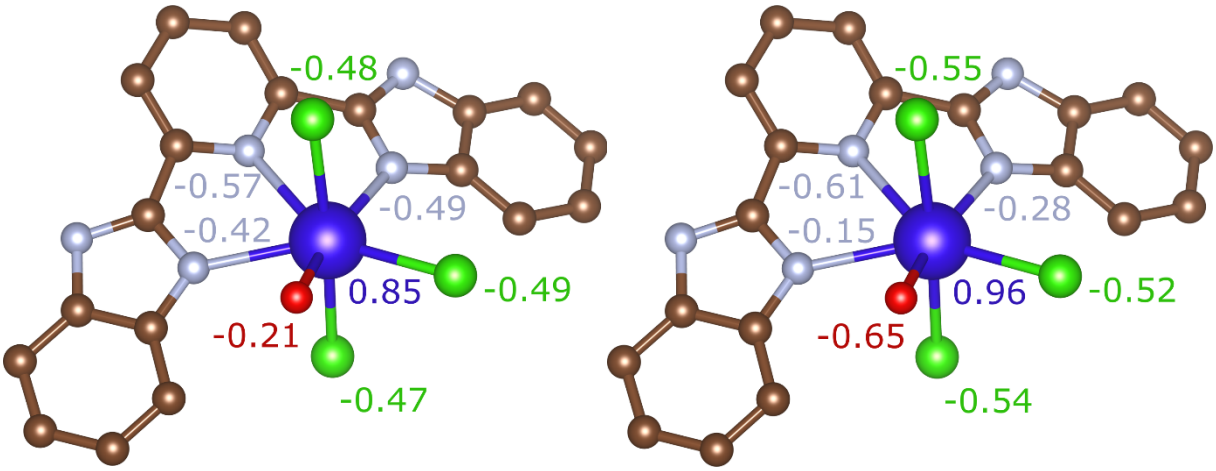

Figure S 16: DFT calculated atomic charges of atoms in coordination sphere of **4** obtained with Mulliken method (left) and CHELPG method (right)¨

Table S 12: Energy level distribution of ground term splitting for complex **5**

E (cm^{-1})
0
4.76
28.59
41.37
83.5
125.02
178.18
191.45
194.11
222.97
243.96
385.3
388.36

S4.2 On the mutual orientation of *D*-tensors in ORCA and PHI

In order to interpret the experimental magnetism of **3**, which is a result of interplay between two non-collinear anisotropic centers, mutual orientation of their *D*-tensors must be taken into account. The quantum chemistry calculation in ORCA provides such information represented by Euler rotation angles which can be subsequently employed in the program PHI. Although both programs use the extrinsic ZY′Z″ convention for rotations, the Euler angles are not necessarily transferable between these two codes. The definition of rotation matrix used in PHI is

$$R^{phi}(\alpha,\beta,\gamma) = R_z(\alpha)R_y(\beta)R_z(\gamma)$$

with

$$R_z(\theta) = \begin{bmatrix} \cos\theta & -\sin\theta & 0 \\ \sin\theta & \cos\theta & 0 \\ 0 & 0 & 1 \end{bmatrix}$$

$$R_y(\theta) = \begin{bmatrix} \cos\theta & 0 & \sin\theta \\ 0 & 1 & 0 \\ -\sin\theta & 0 & \cos\theta \end{bmatrix}$$

and it is employed as premultiplication, i.e. it describes the rotation of the *D*-tensor with respect to the reference frame (*active* rotation). In contrast, the rotation matrix in ORCA describes the rotation of the reference frame with respect to the *D*-tensor (*passive* rotation) and therefore acts as postmultiplication. Thanks to the fortunate parametrization

$$R^{orca}(\alpha,\beta,\gamma) = R_z^{\mathrm{T}}(\gamma)R_y^{\mathrm{T}}(\beta)R_z^{\mathrm{T}}(\alpha)$$

the relation between the two formalisms is still very simple

$$R^{phi} = \left(R^{orca}\right)^{\mathrm{T}}$$

Nevertheless, the rotation matrix in ORCA is constructed as the union of three row-represented eigenvectors of the *D*-tensor and these eigenvectors are lined up so that their corresponding eigenvalues result in equally signed ZFS parameters *D* and *E*. For this sake the first two rows of rotation matrix are sometimes permuted, that is, such a matrix randomly represents proper (i.e. $\det(R^{orca}) = +1$) or improper rotation (i.e. $\det(R^{orca}) = -1$). In the latter case, the declared Euler angles are not transferable to PHI and cannot be used for direct assignment between main axes of *D*-tensor and *g*-tensor. Therefore, rather than using the printed values, the Euler angles were extracted from ORCA rotation matrix (corrected by swapping the *x* and *y* rows for the case of improper rotation) $R^{orca}_{corrected} = \left[a_{ij}\right]$ using the standard formulae

$$\alpha = \arctan\left(\frac{a_{23}}{a_{13}}\right)$$

$$\beta = \arctan\left(\frac{\sqrt{1-a_{33}^2}}{a_{33}}\right)$$

$$\gamma = \arctan\left(\frac{a_{32}}{-a_{31}}\right)$$

Such angles are subsequently consistent with the input of PHI.

S5 Dynamic magnetic investigations

The magnetic data induced by the oscillating; alternating-current (AC) magnetic field were obtained at an amplitude of B_{AC}=0.1 mT. To determine the optimum DC field to suppress the quantum tunnelling of magnetization, AC susceptibility measurements under various DC fields were applied at 2 K (Figure S14). Collected sets of χ' and χ'' at each DC field were fitted using the formulas for extended one-set Debye model

Collected sets of χ' and χ'' (susceptibilities (22 χ' and 22 χ'') at each temperature were fitted using the formulas for extended one-set Debye model (case of **1-3**)

$$\chi'(\omega) = \chi_S + (\chi_T - \chi_S)\frac{1+(\omega\tau)^{(1-\alpha)}\sin(\pi\alpha/2)}{1+2(\omega\tau)^{(1-\alpha)}\sin(\pi\alpha/2)+(\omega\tau)^{(2-2\alpha)}} \quad \textbf{(S1)}$$

$$\chi''(\omega) = (\chi_T - \chi_S)\frac{(\omega\tau)^{(1-\alpha)}\cos(\pi\alpha/2)}{1+2(\omega\tau)^{(1-\alpha)}\sin(\pi\alpha/2)+(\omega\tau)^{(2-2\alpha)}} \quad \textbf{(S2)}$$

or two-set Debye model (case of **4**)

$$\chi'(\omega) = \chi_S + (\chi_{T1} - \chi_S)\frac{1+(\omega\tau_1)^{(1-\alpha_1)}\sin(\pi\alpha_1/2)}{1+2(\omega\tau_1)^{(1-\alpha_1)}\sin(\pi\alpha_1/2)+(\omega\tau_1)^{(2-2\alpha_1)}} + (\chi_{T2} - \chi_{T1})\frac{1+(\omega\tau_2)^{(1-\alpha_2)}\sin(\pi\alpha_2/2)}{1+2(\omega\tau_2)^{(1-\alpha_2)}\sin(\pi\alpha_2/2)+(\omega\tau_2)^{(2-2\alpha_2)}} \quad \textbf{(S3)}$$

$$\chi''(\omega) = (\chi_{T1} - \chi_S)\frac{(\omega\tau_1)^{(1-\alpha_1)}\cos(\pi\alpha_1/2)}{1+2(\omega\tau_1)^{(1-\alpha_1)}\sin(\pi\alpha_1/2)+(\omega\tau_1)^{(2-2\alpha_1)}} + (\chi_{T2} - \chi_{T1})\frac{(\omega\tau_2)^{(1-\alpha_2)}\cos(\pi\alpha_2/2)}{1+2(\omega\tau_2)^{(1-\alpha_2)}\sin(\pi\alpha_2/2)+(\omega\tau_2)^{(2-2\alpha_2)}} \quad \textbf{(S4)}$$

Further temperature-dependent AC susceptibility investigation was conducted at the same field of 0.125 T for **1**-**3**, and 0.08 T for **4**. These investigations were conducted over the temperature ranges of 1.9–3.9 K for compound **1**, 1.9–4.5 K for compound **2** and 1.9–3.1 K for compound **3** and 2.0–2.9 for compound **4**. The collected datasets of χ' and χ'' at each temperature were fitted using the equations for the extended one-set Debye model (eqs. S1 – S4).

Table S13 Parameters of the extended one-set Debye model (eq. S1 and S2) for **1** measured at T = 2.0 K.

B / T	χ_S /10^{-6} cm^3 mol^{-1}	χ_T/10^{-6} cm^3 mol^{-1}	α	τ /ms	R^2
0.005	-	-	-	-	-
0.01	-	-	-	-	-
0.015	-	-	-	-	-
0.02	-	-	-	-	-
0.03	10.31(2)	10.75(2)	0	1.45(6)	0.99989
0.04	9.33(2)	10.71(2)	0.06(2)	1.20(4)	0.9999
0.05	9.33(2)	10.71(2)	0.06(2)	1.20(4)	0.9999
0.06	8.75(2)	10.68(2)	0.09(1)	1.14(3)	0.9999

0.07	8.15(2)	10.66(2)	0.107(1)	1.09(2)	0.9999
0.08	7.55(2)	10.63(2)	0.124(9)	1.04(2)	0.9999
0.09	6.97(2)	10.60(2)	0.137(8)	1.01(1)	0.99989
0.1	6.42(3)	10.57(2)	0.153(7)	1.0(1)	0.99987
0.125	5.17(3)	10.46(2)	0.193(7)	0.9(1)	0.99983
0.15	4.12(4)	10.34(3)	0.236(7)	0.85(12)	0.99976
0.2	2.42(7)	10.20(4)	0.339(8)	0.8(2)	0.99958

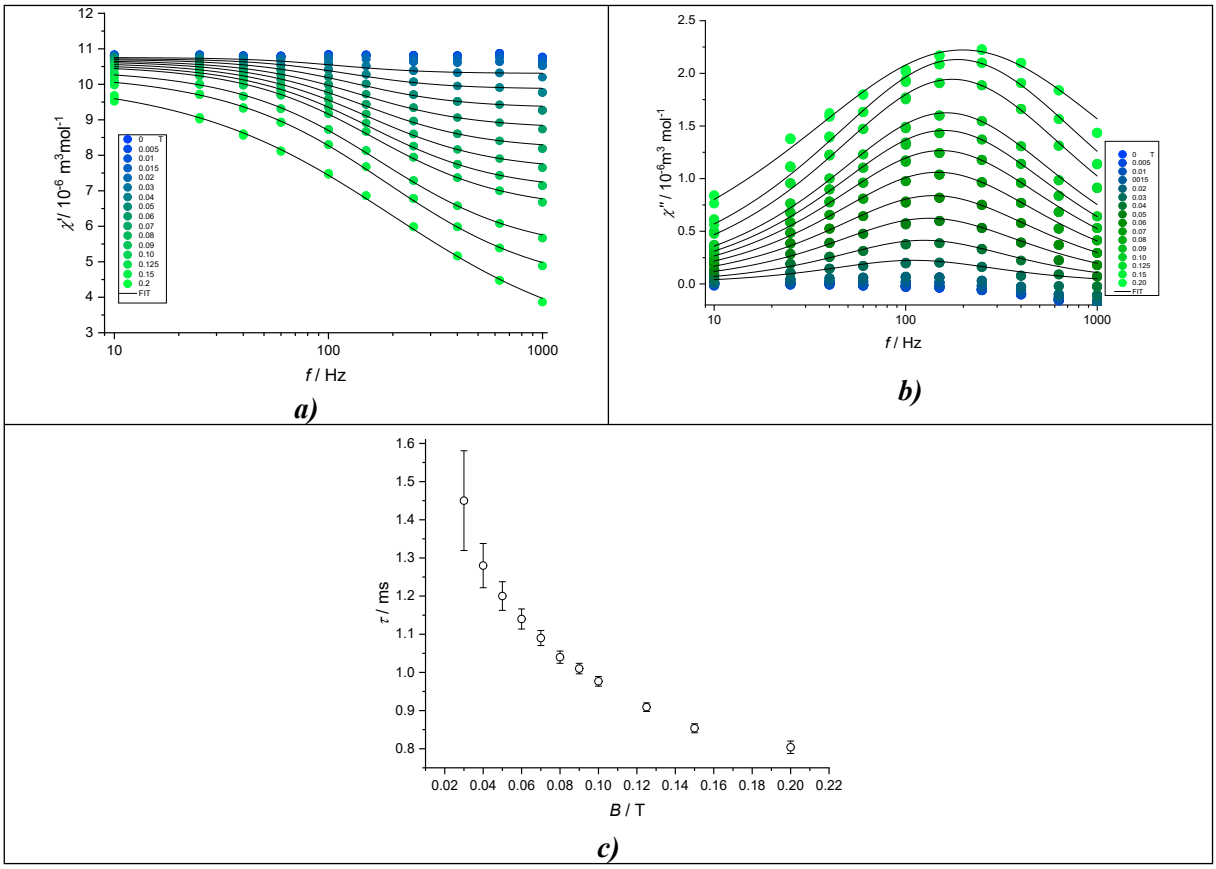

Figure S17 AC susceptibility data for **1** recorded at various static magnetic fields at $T = 2.0$ K: Frequency dependent in-phase χ'(***a***) and out-of-phase χ''(***b***) component of AC susceptibility (solid lines are results of fits according to equations S1 and S2). Field dependency of relaxation time τ with standard errors (***c***).

Table S14 Parameters of the extended one-set Debye model (eq. S1 and S2) for **1** measured at 0.125 T.

T /K	χ_S /10^{-6} cm^3 mol^{-1}	χ_T /10^{-6} cm^3 mol^{-1}	α	τ / ms	R^2
1.9	5.42(5)	11.03(2)	0.215(9)	1.01(2)	0.99965
2.1	4.82(5)	10.18(1)	0.219(8)	0.85(2)	0.99975
2.3	4.40(7)	9.44(2)	0.21(1)	0.85(2)	0.99975
2.5	4.05(9)	8.83(2)	0.19(1)	0.59(2)	0.99909
2.7	3.81(6)	8.25(1)	0.17(1)	0.50(1)	0.99962
2.9	3.57(5)	7.76(1)	0.157(9)	0.42(97)	0.99973

3.1	3.39(4)	7.330(7)	0.146(7)	0.36(6)	0.99985
3.3	3.24(7)	6.948(9)	0.13(1)	0.30(9)	0.99968
3.5	3.14(5)	6.598(5)	0.116(7)	0.25(5)	0.99987
3.7	3.09(7)	6.265(6)	0.09(1)	0.21(7)	0.99978
3.9	3.02(10)	5.987(8)	0.07(2)	0.17(8)	0.99965

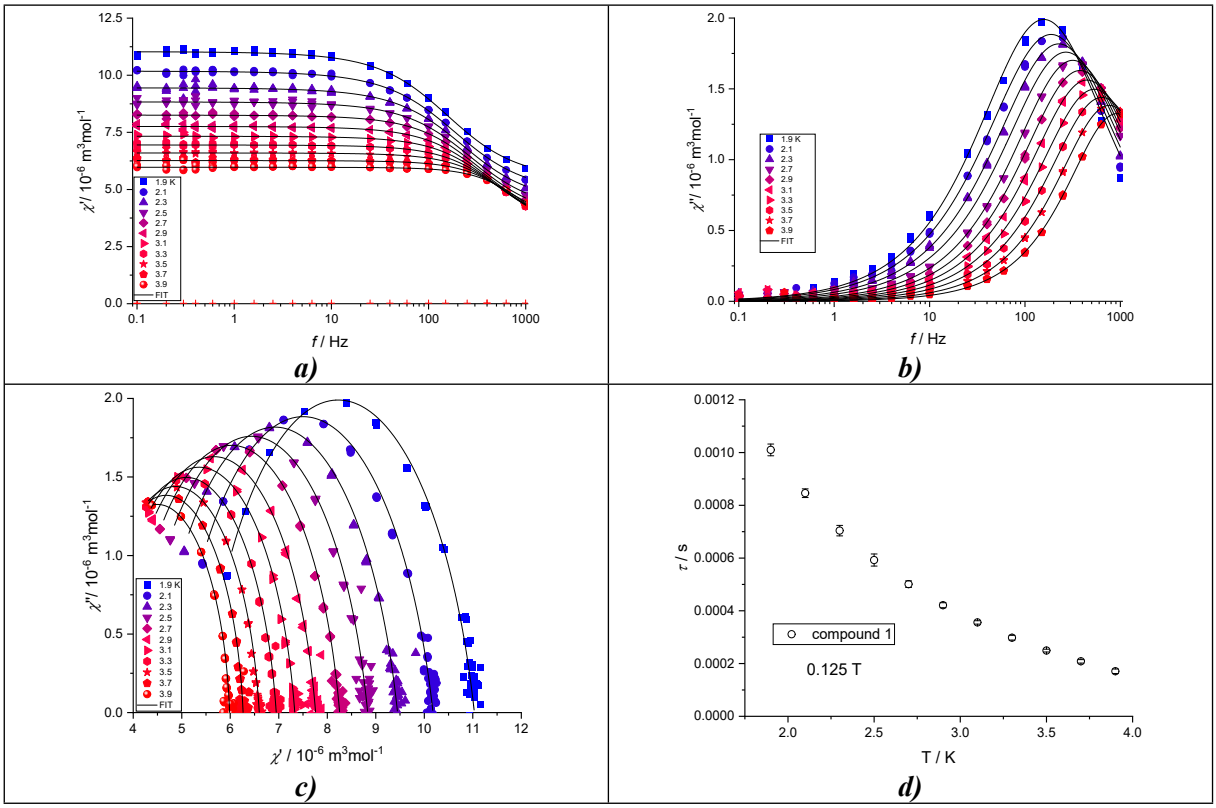

Figure S18 AC susceptibility data for **1** recorded at B_{DC}=0.125 T in temperature range 1.9-3.9 K: Frequency dependent in-phase χ'(***a***) and out-of-phase χ''(***b***) component of AC susceptibility and Cole-Cole diagram (***c***) (solid lines are results of fits according to equations S1 and S2). Relaxation time τ as function of temperature (***d***).

Table S15 Parameters of the extended one-set Debye model (eq. S1 and S2) for **2** measured at T = 2.0 K.

B **/ T**	χ_S **/10^{-6} cm^3 mol^{-1}**	χ_T**/10^{-6} cm^3 mol^{-1}**	***α***	***τ*** **/ms**	R^2
0.005	-	-	-	-	-
0.01	-	-	-	-	-
0.15	-	-	-	-	-
0.02	-	-	-	-	-
0.03	10.65(1)	11.14(2)	0	2.5(2)	0.99989
0.04	10.19(2)	11.14(3)	0.06(3)	2.3(1)	0.9999
0.05	9.64(2)	11.12(3)	0.08(2)	2.1(7)	0.9999
0.06	9.03(2)	11.09(3)	0.10(5)	1.97(5)	0.9999
0.07	8.41(2)	11.07(3)	0.11(1)	1.86(3)	0.99989
0.08	7.80(2)	11.02(2)	0.118(9)	1.75(3)	0.99989

0.09	7.20(2)	11.01(2)	0.137(7)	1.68(2)	0.9999
0.1	6.64(2)	10.96(2)	0.137(6)	1.6(1)	0.9999
0.125	5.38(2)	10.85(2)	0.156(5)	1.45(1)	0.9999
0.15	4.35(2)	10.66(2)	0.174(5)	1.31(12)	0.99984
0.2	2.76(4)	10.28(4)	0.231(7)	1.08(1)	0.99957

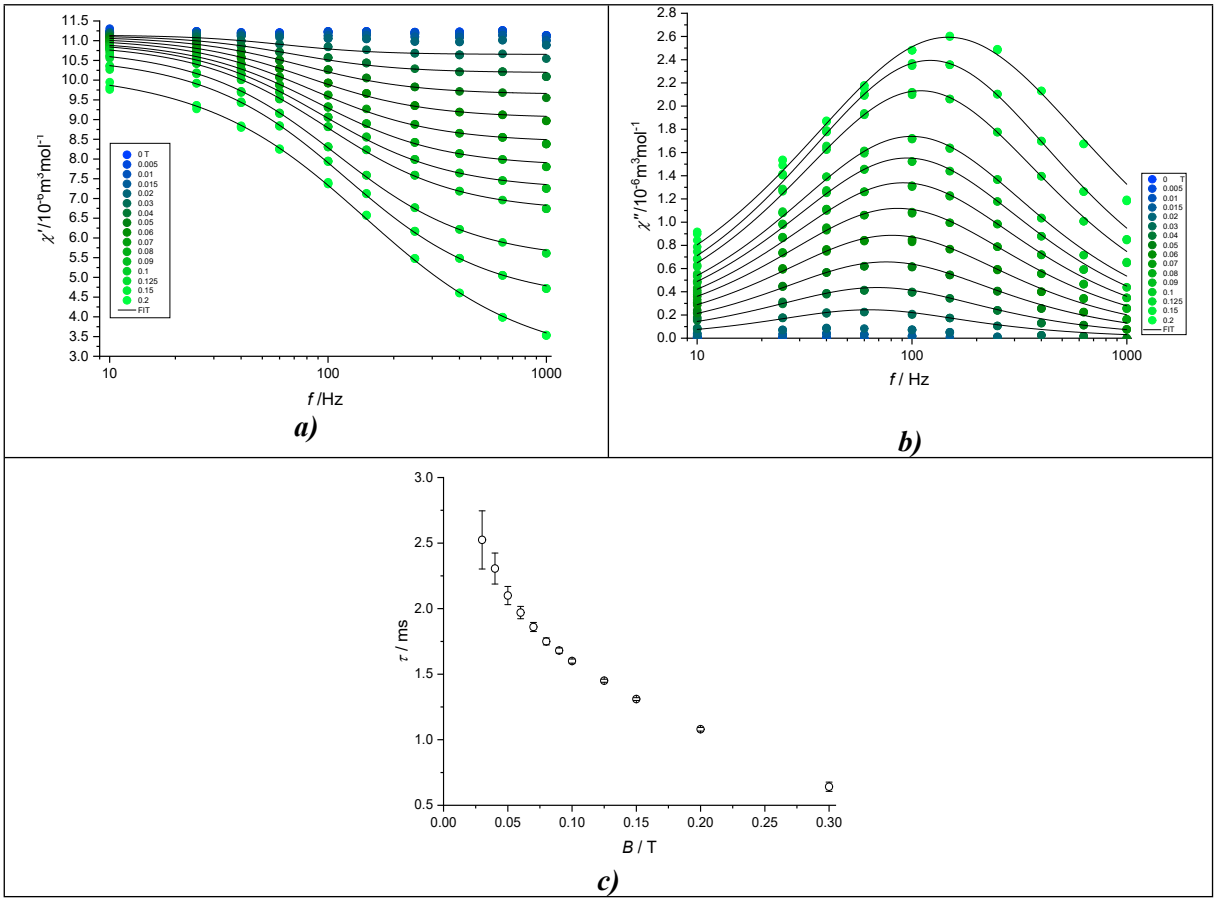

Figure S19 AC susceptibility data for **2** recorded at various static magnetic fields at $T = 2.0$ K: Frequency dependent in-phase χ'(***a***) and out-of-phase χ''(***b***) component of AC susceptibility (solid lines are results of fits according to equations S1 and S2). Relaxation time τ as function of static magnetic field B_{DC} (***c***)

Table S16 Parameters of the extended one-set Debye model (eq. S1 and S2) for **2** measured at 0.125 T.

T **/K**	χ_S **/10^{-6} cm^3 mol^{-1}**	χ_T **/10^{-6} cm^3 mol^{-1}**	***α***	***τ*** **/ms**	**R²**
1.9	5.88(9)	11.85(4)	0.16(2)	1.63(5)	0.9985
2.1	5.21(6)	10.98(2)	0.178(1)	1.39(3)	0.99936
2.3	4.79(6)	10.16(2)	0.15(1)	1.17(3)	0.99934
2.5	4.45(6)	9.45(2)	0.13(1)	0.98(2)	0.99918
2.7	4.15(3)	8.83(1)	0.114(8)	0.81(1)	0.99968
2.9	3.87(6)	8.35(2)	0.11(1)	0.66(1)	0.99939
3.1	3.67(5)	7.85(1)	0.092(7)	0.52(1)	0.99961
3.3	3.49(6)	7.44(1)	0.08(1)	0.4(1)	0.9995

3.5	3.33(7)	7.07(1)	0.07(1)	0.30(8)	0.99957
3.7	3.24(7)	6.719(8)	0.05(1)	0.22(6)	0.99974
3.9	3.2(1)	6.421(8)	0.07(2)	0.17(8)	0.99965
4.1	3.2(1)	6.130(7)	0.02(2)	0.13(7)	0.99974
4.3	3.2(1)	5.875(6)	0.01(2)	0.10(7)	0.99981
4.5	3.3(1)	5.637(6)	0	0.80(4)	0.99977

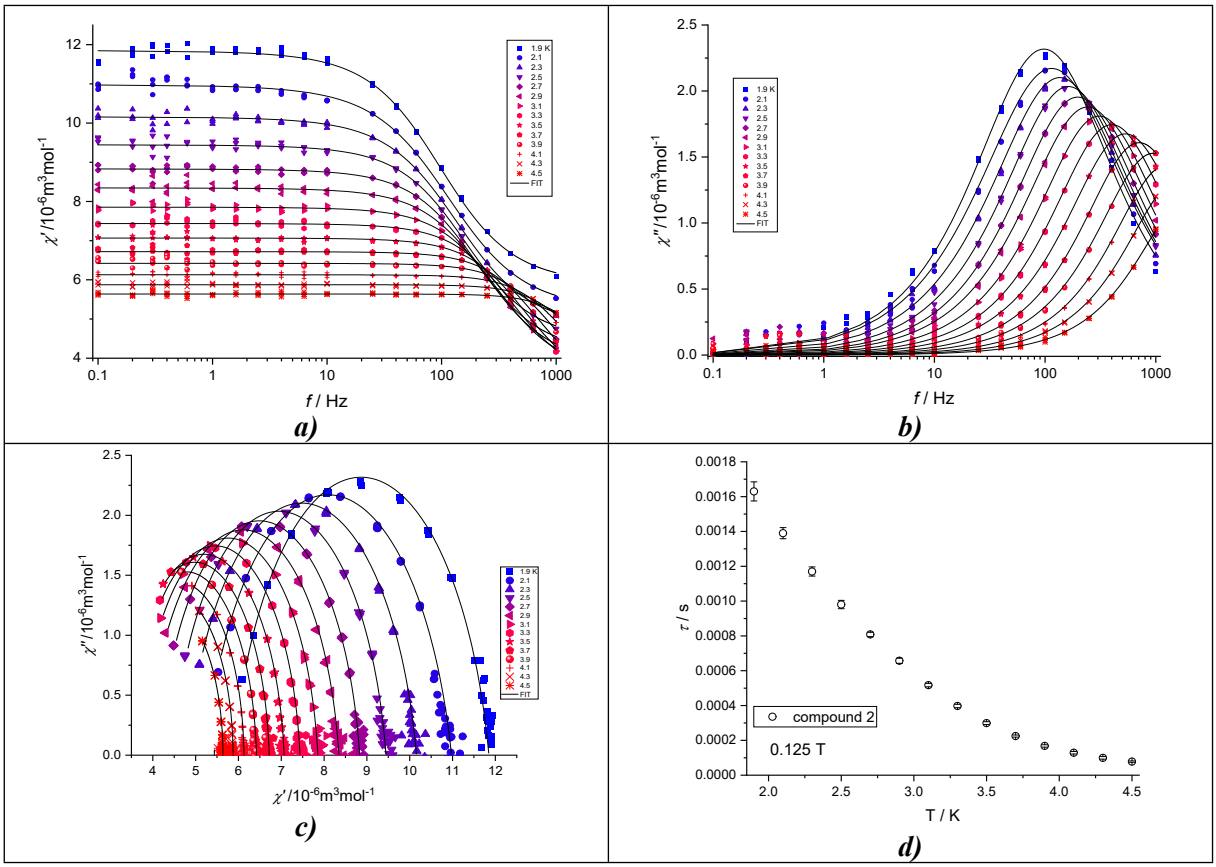

Figure S20 AC susceptibility data for **2** recorded at B_{DC}=0.125 T in temperature range 1.9-5.7 K: Frequency dependent in-phase χ'(***a***) and out-of-phase χ''(***b***) component of AC susceptibility and Cole-Cole diagram (***c***) (solid lines are results of fits according to equations S1 and S2). Relaxation time τ as function of temperature (***d***).

Table S17 Parameters of the extended one-set Debye model (eq. S1 and S2) for **3** measured at T = 2.0 K.

B **/ T**	χ_S **/10^{-6} cm^3 mol^{-1}**	χ_T **/10^{-6} cm^3 mol^{-1}**	α	τ **/ms**	**R^2**
0.005	-	-	-	-	-
0.01	8.90(2)	10.62(1)	0.055(11)	1.15(2)	0.99995
0.015	6.96(1)	10.71(1)	0.113(5)	1.38(1)	0.99995
0.02	5.42(2)	10.82(2)	0.145(5)	1.69(1)	0.99987
0.03	3.56(1)	10.97(4)	0.182(6)	2.22(2)	0.99956
0.04	2.59(3)	11.09(6)	0.202(7)	2.61(3)	0.99922
0.05	2.02(2)	11.20(6)	0.219(6)	2.86(4)	0.99922

0.06	1.69(3)	11.20(6)	0.223(6)	2.99(4)	0.99908
0.07	1.48(7)	11.20(7)	0.225(1)	3.08(4)	0.99894
0.08	1.33(4)	11.18(7)	0.225(7)	3.13(4)	0.99889
0.09	1.22(4)	11.16(7)	0.225(6)	3.16(4)	0.99889
0.1	1.13(4)	11.19(7)	0.228(7)	3.21(5)	0.999877
0.125	0.99(4)	11.05(8)	0.225(5)	3.2(5)	0.99861
0.15	0.90(4)	10.96(8)	0.223(7)	3.2(5)	0.99984
0.2	0.80(5)	10.62(9)	0.220(8)	3.11(5)	0.99806
0.3	0.69(5)	10.05(9)	0.237(9)	2.94(6)	0.99769
0.4	0.53(6)	9.6(1)	0.30(1)	2.87(7)	0.99741

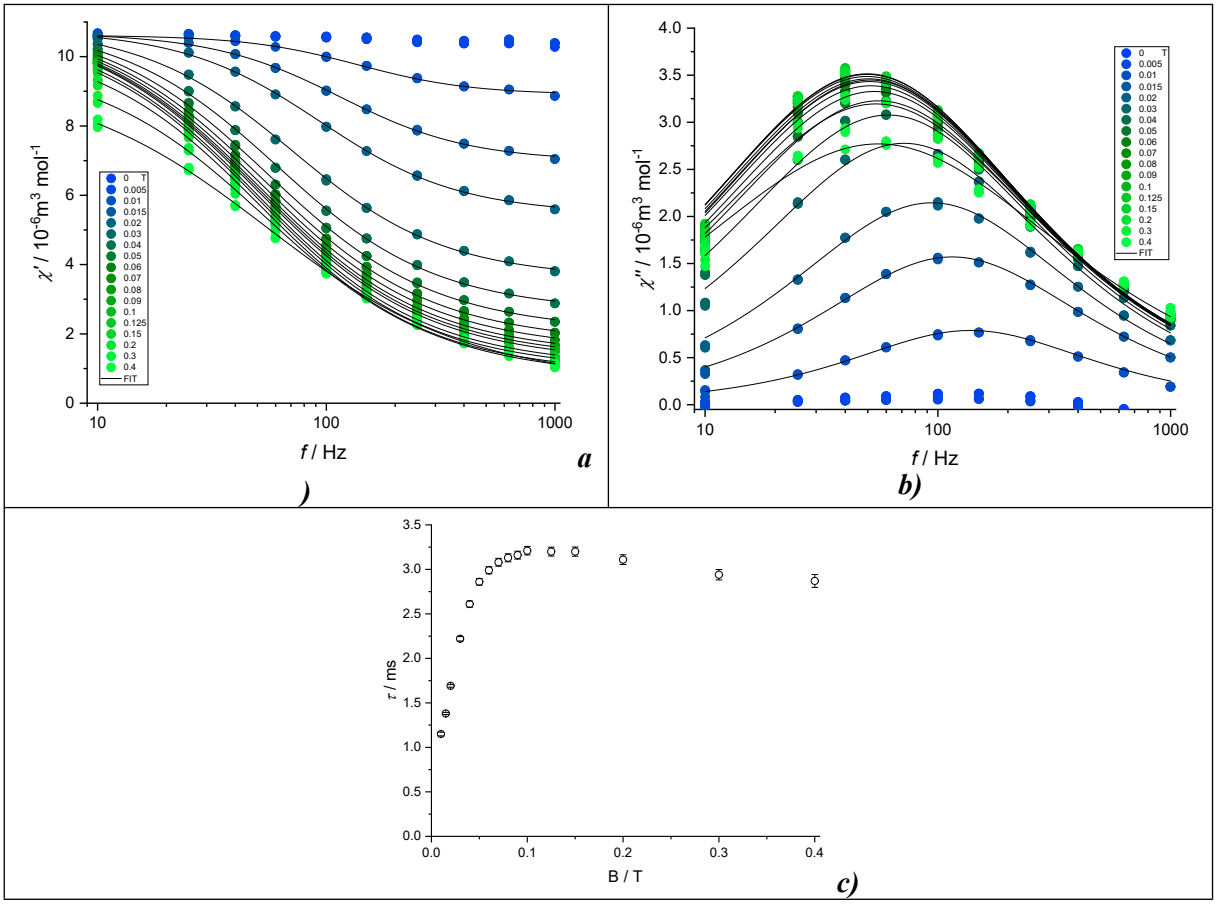

Figure S21 AC susceptibility data for **3** recorded at various static magnetic fields at $T = 2.0$ K: Frequency dependent in-phase χ'(***a***) and out-of-phase χ''(***b***) component of AC susceptibility (solid lines are results of fits according to equations S1 and S2). Relaxation time τ as function of static magnetic field B_{DC} (***c***)

Table S18 Parameters of the extended one-set Debye model (eq. S1 and S2) for **3** measured at 0.125 T.

T /K	χ_S /10^{-6} cm^3 mol^{-1}	χ_T/10^{-6} cm^3 mol^{-1}	α	τ / ms	R^2
1.9	1.20(5)	11.20(3)	0.184(7)	3.55(5)	0.99885
2.1	1.13(4)	10.15(3)	0.172(6)	2.48(3)	0.99911

2.3	1.08(4)	9.27(2)	0.143(5)	1.58(2)	0.9994
2.5	1.02(3)	8.57(1)	0.108(4)	0.90(7)	0.99972
2.7	0.93(3)	7.949(8)	0.078(3)	0.45(3)	0.99982
2.9	0.91(4)	7.393(5)	0.055(3)	0.22(2)	0.99992
3.1	0.9(1)	1.07(4)	0.063(8)	0.11(4)	0.99985

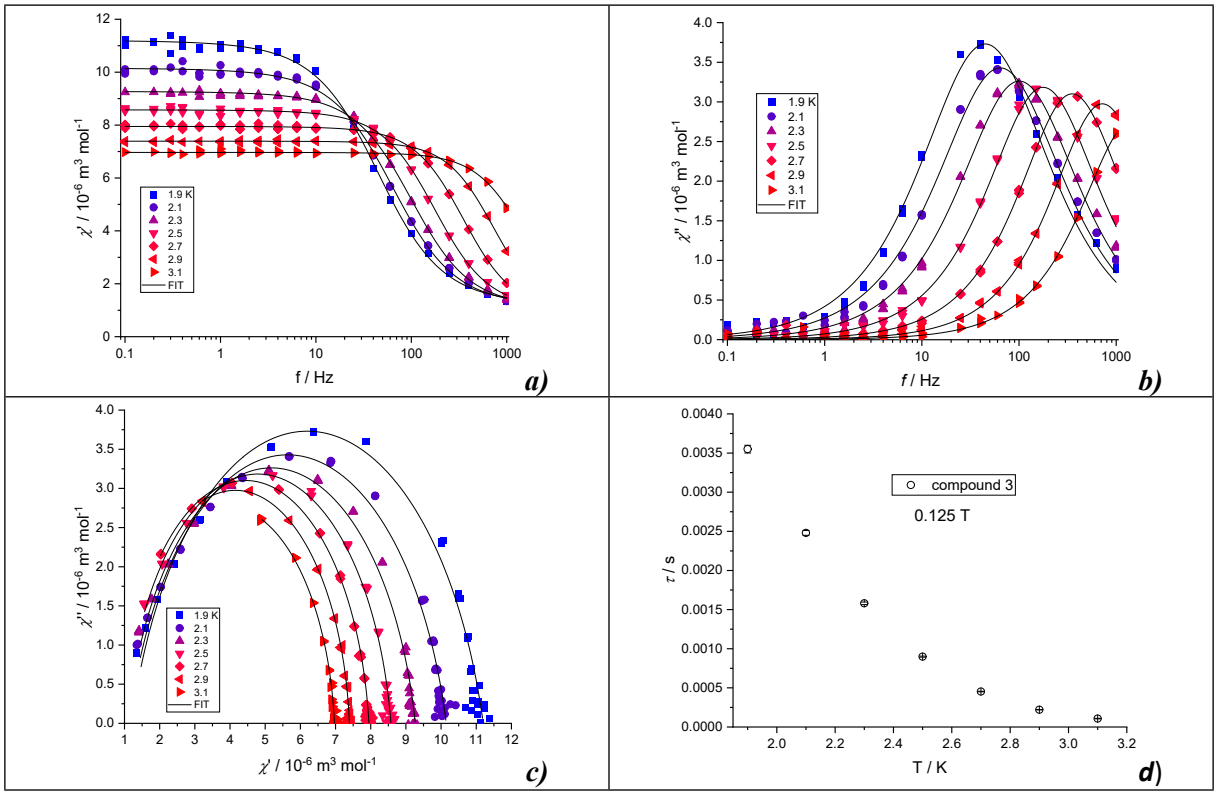

Figure S22 AC susceptibility data for **3** recorded at B_{DC}=0.125 T in temperature range 1.9-3.1 K: Frequency dependent in-phase χ'(***a***) and out-of-phase χ''(***b***) component of AC susceptibility (solid lines are results of fits according to equations S1 and S2). Relaxation time τ as function of temperature (***c***)

Table S19 Parameters of the extended one-set Debye model (eq. S3 and S4) for **4** measured at T = 2.0 K.

B / **T**	χ_S /10^{-6} m^3 mol^{-1}	$\chi_{T,1}$ /10^{-6} m^3 mol^{-1}	$\chi_{T,2}$ /10^{-6} m^3 mol^{-1}	α_1	α_2	τ_1 / ms	τ_2 / ms	R^2
0	-	-	-	-	-	-	-	-
0.02	62(2)	81.9(3)	80.1(7)	0.09(4)	0.3(3)	0.13(1)	0.3(3)	0.99985
0.04	38.1(4)	81.7(2)	83.1(1)	0.163(7)	0.2(1)	0.195(3)	0.07(2)	0.99998
0.06	24.1(4)	78.8(3)	82.4(1)	0.212(6)	0.31(6)	0.242(3)	0.049(8)	0.99998
0.08	17.8(5)	74.5(6)	81.2(2)	0.23(1)	0.34(5)	0.283(4)	0.040(7)	0.99996
0.1	13.0(4)	67.5(9)	80.2(2)	0.24(1)	0.44(5)	0.283(4)	0.026(5)	0.99998
0.12	10.4(6)	62(1)	77.9(2)	0.26(1)	0.41(3)	0.286(6)	0.027(4)	0.99995
0.14	9.8(8)	56(1)	76.1(3)	0.25(2)	0.40(3)	0.284(9)	0.028(4)	0.9999

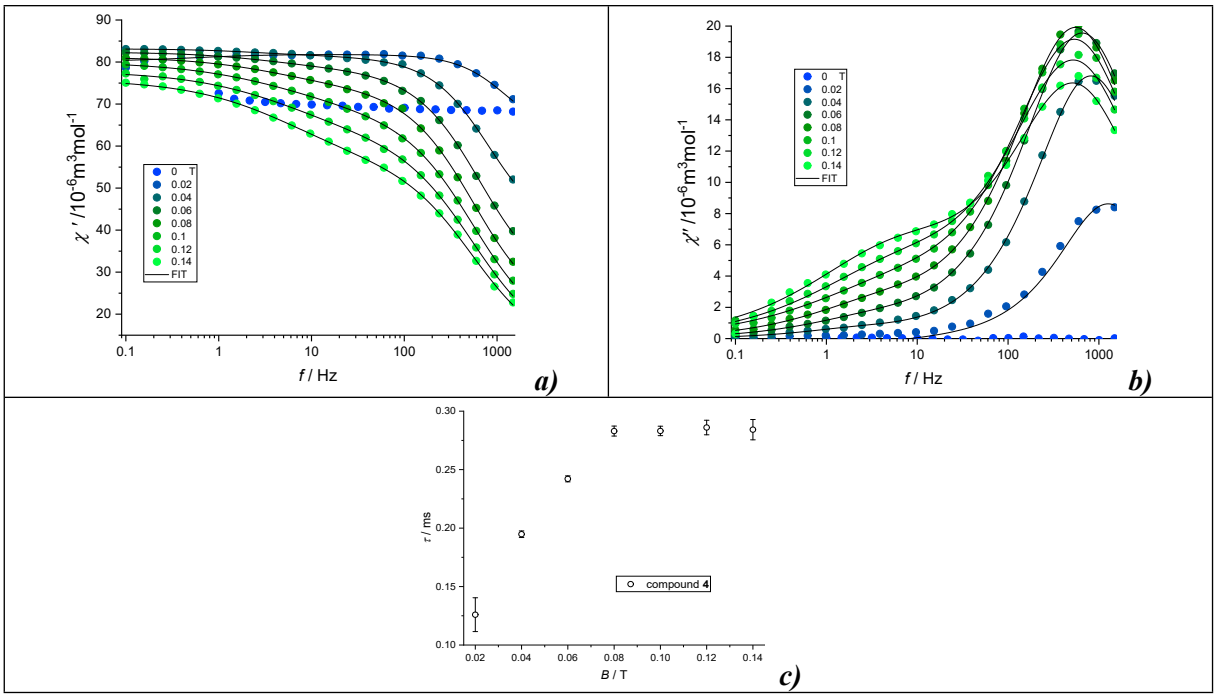

Figure S23 AC susceptibility data for **4** recorded at various static magnetic fields at $T = 2.0$ K: Frequency dependent in-phase χ'(***a***) and out-of-phase χ''(***b***) component of AC susceptibility (solid lines are results of fits according to equations S3 and S4). Relaxation time τ as function of static magnetic field B_{DC} (***c***)

Table S20 Parameters of the extended two-set Debye model (eq. S3 and S4) for **4** measured at 0.08 T.

T /K	χ_S /10^{-6} m^3 mol^{-1}	$\chi_{T,1}$ /10^{-6} m^3 mol^{-1}	$\chi_{T,2}$ /10^{-6} m^3 mol^{-1}	α_1	α_2	τ_1 / ms	τ_2 / s	R^2
2.0	17.2(3)	74.7(3)	80.9(2)	0.248(5)	0.26(4)	0.288(2)	0.037(3)	0.99998
2.1	17.7(4)	70.8(5)	77.9(3)	0.235(8)	0.34(5)	0.219(3)	0.032(3)	0.99997
2.2	18.4(6)	67.5(5)	74.6(3)	0.23(1)	0.33(5)	0.172(3)	0.024(3)	0.99996
2.3	19.2(6)	66.9(6)	73.8(3)	0.21(1)	0.37(6)	0.160(3)	0.024(3)	0.99996
2.4	20.9(8)	63.2(5)	69.5(2)	0.20(1)	0.36(5)	0.115(3)	0.015(3)	0.99997
2.5	21.6(9)	61.2(4)	67.1(2)	0.20(1)	0.39(5)	0.091(3)	0.016(1)	0.99998
2.6	21(1)	59.1(5)	64.7(2)	0.21(2)	0.41(5)	0.067(4)	0.013(2)	0.99998
2.7	21(1)	57.6(4)	62.6(1)	0.23(2)	0.42(4)	0.049(3)	0.014(2)	0.99999
2.8	17(3)	56.4(4)	60.5(2)	0.29(2)	0.42(5)	0.031(4)	0.016(2)	0.99999
2.9	15(5)	55.0(4)	58.5(1)	0.32(3)	0.40(5)	0.021(5)	0.016(3)	0.99999

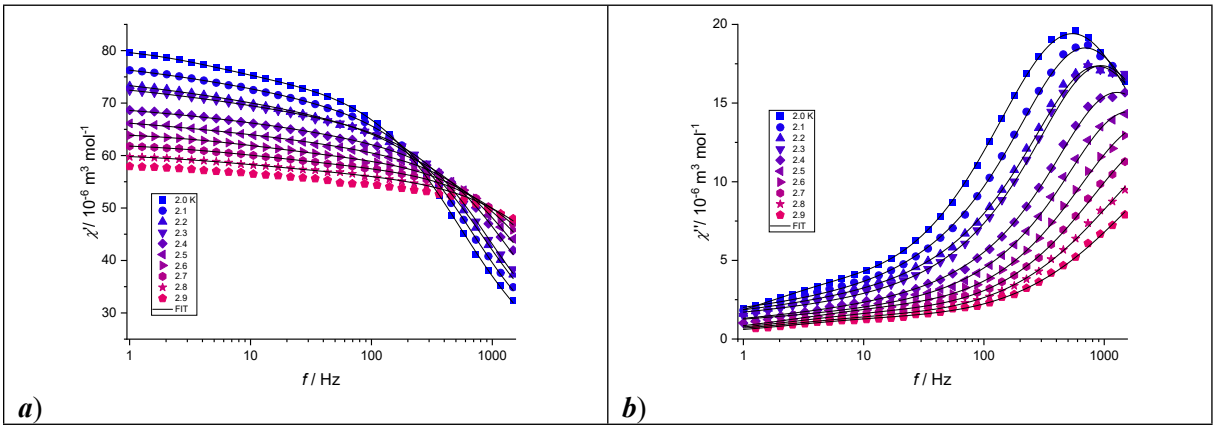

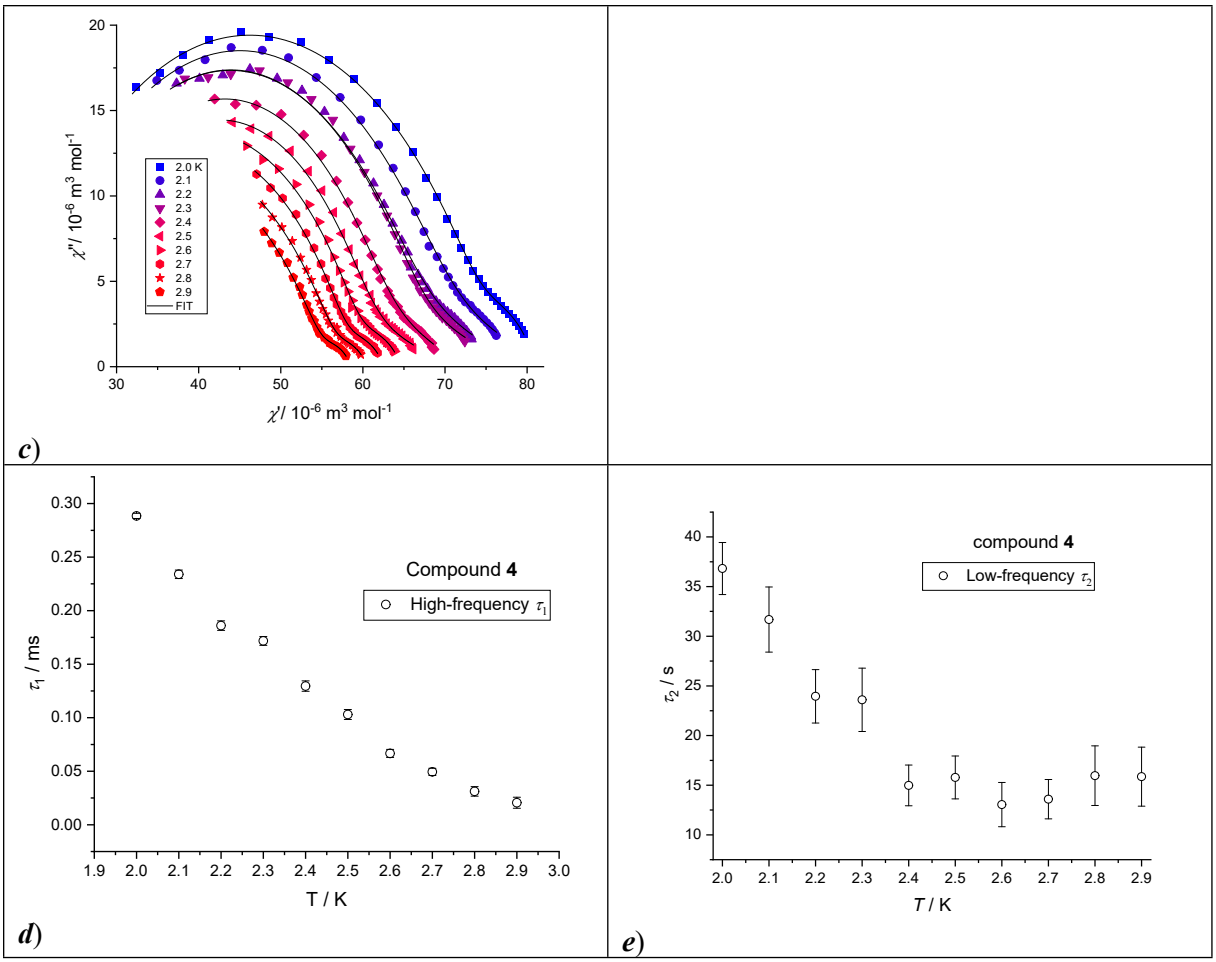

Figure S24 AC susceptibility data for **4** recorded at B_{DC}=0.08 T in temperature range 2.0-2.9 K: Frequency dependent in-phase χ'(***a***) and out-of-phase χ''(***b***) component of AC susceptibility and Cole-Cole diagram (***c***) (solid lines are results of fits according to equations S3 and S4). (***d***, ***e***) Relaxation times τ as function of temperature.

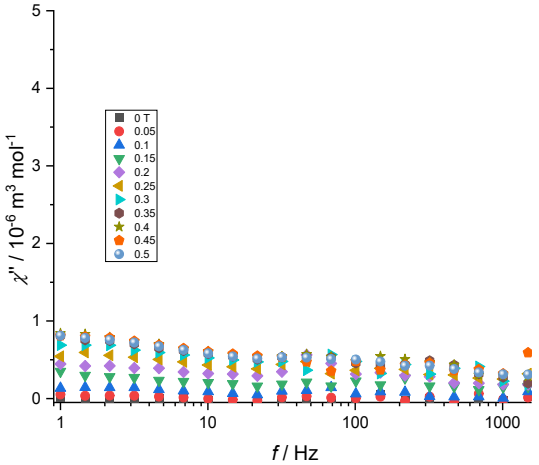

Figure S25 Out-of-phase component of AC susceptibility for **5** recorded at T=2 T

Table S 21 Relaxation parameters of reported compounds using the respective combinations of Orbach, Raman and Direct relaxation processes.

	U/k_B/ K	τ_0/ s	C / K^{-n} s^{-1}; n	AB^m/ K^{-1} s^{-1}	R^2
Compound **1**					
Raman+direct	-	-	10(2) 4.4(1)	436(12)	0.99968
Orbach+direct	15.9(7)	$4.6(9)\times10^{-6}$		510(13)	0.99837
Orbach for 3.3 − 3.9 K	11.9(6)	$8(1)\times10^{-6}$			0.99149
Compound **2**					
Raman+direct	-	-	0.63(7) 6.54(7)	303(4)	0.99975
Orbach+direct	25.0(5)	$3.5(5)\times10^{-7}$	-	340(6)	0.99905
Orbach for 3.7 − 4.5 K	22.0(3)	$6.0(5)\times10^{-7}$	-	-	0.99918
Compound **3**					
Raman+direct	-	-	0.030(6) 11.1(2)	132(4)	0.99962
Raman+direct*	-	-	failed	1071(156)	0.98285
Orbach+direct	31(1)	$5(2)\times10^{-9}$	-	149(8)	0.99794
Orbach for 2.5 − 3.1 K	27(1)	$1.7(9)\times10^{-8}$	-	-	0.99141
Compound **4**					
Raman+direct	-	-	0.13(12) 11.9(9)	1678(161)	0.99241
Raman+direct*	-	-	2.5 (2) 9 fixed	1071(156)	0.98285
Orbach+direct	33(3)	$3(3)\times10^{-10}$	-	1834(151)	0.9900
Orbach for 3.7 − 4.5 K	30(2)	$7(6)\times10^{-10}$	-	-	0.98123

*n fixed to theoretical value 9

S6 Magneto-structural correlations

Table S22 Pentacoordinate complexes [Co(Rbbp)X_2] with chlorido (green, X=Cl) and bromido (brown, X=Br) terminal ligands.

	SHAPE analysis[i] τ_5	**Magnetic anisotropy**[ii] (cm^{-1})	τ (ms) [iii]	U_{eff} (K)[iv]
[Co(C8bbp)Cl_2][29]	S(SPY)= 2.4 S(TBPY)= 3.5 τ_5 = 0.18	D= −69[m]; (−61.7[a]) E/D= 0[m]; (0.26[a]) Δ_{ax}= −3153[m] Δ_{rh}= −8[m]	τ= 23.3 @2.0K and 0.1T	33.0 @0.1T
[Co(C8bbp)Br_2][29]	S(SPY)= 2.1 S(vOC)= 4.1 τ_5= 0.13	D= −43[m]; (+48.8[a]) E/D= 0[m]; (0.25[a]) Δ_{ax}= −329[m] Δ_{rh}= −99[m]	τ= 1.6 @2.0K and 0.1T	27.0 @0.1T
δ^{ClBr}= 34.1°; τ(Cl)/τ(Br)=14.6				
[Co(C10bbp)Br_2][30]	S(SPY)= 2.5 S(vOC)= 4.8 τ_5 = 0.04	Δ_{ax}= −1503[m](−1508[a]) Δ_{rh}= −270 [m](−164[a])	τ= 19.8 @2.0K and 0.1T	34.0 @0.06T
[Co(C12bbp)Cl_2][29]	S(SPY)=2.2 S(TBPY)= 4.7 S(vOC)= 4.8	D= −78[m]; (−91.4[a]) E/D= 0[m]; (0.16[a])	τ=72.7 @2.0K and 0.1T	37.0 @0.1T

	τ_5 = 0.12	Δ_{ax}= −1952[m] Δ_{rh}= −0[m]		
[Co(C12bbp)Br$_2$][29]	*S*(SPY)=2.6 *S*(TBPY)=4.8 *S*(vOC)=4.9 τ_5= 0.08	Δ_{ax}= −2378[m] Δ_{rh}= −82[m]	τ= 9.33 @2.0K and 0.1T	31 @0.1T
δ^{ClBr}= 5.1°; τ(Cl)/τ(Br)=7.8				
[Co(bbp)Cl$_2$]·MeOH[31]	*S*(SPY)= 1.7 *S*(vOC)= 3.2 τ_5 = 0.24	*D*= +14.5[m] *E*/*D*= 0[m]	τ= 0.6 (estimated) @2.0K and 0.1T	19.6 @0.1T
[Co(bbp)Br$_2$]·MeOH[31]	*S*(SPY)=2.2 *S*(vOC)=3.8 τ_5= 0.27	*D*= +8.4[m] *E*/*D*= 0[m]	τ= 4.8 (estimated) @2.0K and 0.125T	8.2 @0.1T
δ^{ClBr}= 17.5°; τ(Cl)/τ(Br)=0.125				
[Co(bbp)Cl$_2$]·DMF[32]	S(SPY)= 1.7 *S*(vOC)= 3.7 τ_5= 0.00	Δ_{ax}= –650[m] Δ_{rh}= 200[m]	τ= 0.28 @2.0K and 0.2T	18.6 @0.2T
[Co(bbp)Br$_2$]·DMF[32]	*S*(SPY)=2.1 *S*(vOC)=4.3 τ_5 = 0.01	Δ_{ax}= −229[m] Δ_{rh}= 48[m]	τ= 0.145 @2.0K and 0.2T	12.7 @0.2T
δ^{ClBr}= 4.7°; τ(Cl)/τ(Br)=1.9				
[Co(tBuBzbbp)Cl$_2$][33]	*S*(TBPY)= 2.0 *S*(SPY)= 4.9 τ_5= 0.5	*D*= +26[m]; (+48[a]) *E*/*D*= 0.33[m]; (0.12[a])	τ= 0.48 @2.0K and 0.15T	12.8 @0.15T
[Co(tBuBzbbp)Br$_2$][33]	*S*(TBPY)=2.5 *S*(SPY)=4.9 τ_5=0.4	*D*= +39[m]; (+49.1[a]) *E*/*D*= 0.33[m]; (0.23[a])	τ= 0.6 @2.0K and 0.125T	14.9 @0.125T
δ^{ClBr}= 16.5°; τ(Cl)/τ(Br)=0.8,				
[Co(L)Cl$_2$] **1**, this work	*S*(SPY)= 2.2 *S*(TBPY)= 4.0 *S*(vOC)= 4.6 τ_5 = 0.31	Δ_{ax}= –165[m] Δ_{rh}= –2.6[m]	τ= 1.0 @2.0K and 0.1T	11.9 @0.125T
[Co(L)Br$_2$] **2**, this work	*S*(SPY)= 2.8 *S*(TBPY)=4.3 τ_5= 0.27	Δ_{ax}= −139[m] Δ_{rh}= −32[m]	τ= 1.6 @2.0K and 0.1T	22.0 @0.125T
δ^{ClBr}= 11.5°; τ(Cl)/τ(Br)=0.63				

[i]the lowest relevant symmetry measure parameters; [ii] magnetic anisotropy described by **SH** or **GFH** parameters, depending on the electronic structure of investigated system; [iii]highest observed relaxation time at 2 K and given B_{DC} field; [iv]obtained from Arrhenius-like fit of high temperature region of lnτ vs. 1/*T*; [a]*ab initio* calculations; [m]magnetic experiments; δ^{ClBr} = similarity parameter calculated as a sum of the differences between 10 corresponding angles of two pentacoordinate polyhedra; **C8bbp** = 2,6-bis(1-octyl-1*H*-benzimidazol-2-yl)-pyridine; **C10bbp** = 2,6-bis(1-decyl-1*H*-benzimidazol-2-yl)-pyridine; **C12bbp** = 2,6-bis(1-dodecyl-1*H*-benzimidazol-2-yl)-pyridine; **bbp** = 2,6-bis(1*H*-benzimidazole-2-yl)pyridine, **tBuBzbbp**=2,6-Bis(1-(3,5-di-tert-butylbenzyl)-1*H*-benzimidazol-2-yl)pyridine, **L**=2,6-bis(3-methoxypropyl-1*H*-benzimidazol-2-yl)pyridine.

Table S23 Heptacoordinate pentagonal-bipyramidal Co(II) complexes

	PBPY-7 δ_{eq} **Axial angle**	***D*(cm^{-1}); E/D**	τ **(ms)** [iii] U_{eff} **(K);** τ_0**(s)**
[Co(pypzbeyz)(NCS)$_2$(DMF)][34]	0.428 18.76 177.2	+36.8; 0.01[m] +33.5; 0.06[N]	3.27 (@1.8 K,0.1T) 29.5; 4.0×10^{-7} [O] 55.9; 2.2×10^{-10} [OR]
[Co(H$_2$L1)(NCS)$_2$](SCN)$_2$.2H$_2$O[35]	0.527 12.7 169.0	+30.0; 0[m] +41.5; 0.05[N]	not measured

$[Co(H_2L1)(NCS)_2][Co(NCS)_4].2H_2O$[35]	0.283 9.9 173.1	+36.6; 0.03^m +38.4; 0.03^N	not measured
$[Co(H_2daps)(MeOH)_2]$[36]	0.235 20.6 176.7	+43.1; 0^m +38.0; 0.09^N	- (@ 0.1 T) 33.5; 7.4×10^{-6} OR
$[Co(H_4daps)(NCS)(MeOH)]\cdot(ClO_4)\cdot(MeOH)$[36]	0.211 14.44 172.6	+41.5; 0^m +38.0; 0.03^N	- (@ 0.1 T) 28.4; 5.6×10^{-6} OR
$[Co(H_4daps)(NCS)_2]\cdot(MeOH)_2$[36]	0.464 12.2 177.9	+38.8; 0^m +37.9; 0.07^N	- (@ 0.1 T) 23.6; 4.8×10^{-6} OR
$[Co(L2)](ClO_4)_2$[37]	0.94/0.94 5.1/5.6 174.0/174.7	+34.0; 0^m +30.6; 0.04^N	0.003 (@1.9K; 0.1 T) no maximum of χ''
$[Co(L3)](ClO_4)_2$[38]	0.5 6.75 176.1	+40.0; 0^m +45.0; 0.04^N	not measured
$[Co(H_2dapb)(H_2O)(NO_3)](NO_3)$[39,40]	0.417 12.9 173.4	+32.4; 0^m +35.5; 0.07^N	10.45 (@2 K,0.1T) 81.2; 6.0×10^{-10}
$[Co(L4)(H_2O)_2]Cl_2\cdot4H_2O$[39,40]	0.289 7.3 176.1	+24.6; 0^m +35.15; 0.02^N	16.05 (@2 K,0.1T) 29.8;1.2×10^{-6}
$[Co(dapb)(im)_2]\cdot H_2O$[39,40]	0.364 19.1 175.0	+24.8; 0^m +35.0; 0.06^N	20.5 (@2 K,0.1T) 89.6; 8.7×10^{-11} O
$[Co(dapbh)(H_2O)(CH_3OH)]$[41]	0.197 11.6 178.4	+27.0; 0^m +37.3; 0.05^N	30 (@2.4 K,0.2T) 12.25; 4.24×10^{-4} O 22.16; 9.69×10^{-5} OD
$[Co(Hdapbh)(N_3)(CH_3OH)]\cdot(CH_3OH)$[41]	0.285 7.41 177.4	+21.9; 0^m +37.3; 0.08^N	0.3 (@2.0 K,0.2T) 27.5; 4.0×10^{-7} O 44.15; 4.0×10^{-8} OD
$[Co(H_2aapbh)(CH_3OH)_2]\cdot(NO_3)_2$[41]	0.104 9.8 177.3	+31.9; 0^m +41.1; 0.06^N	no maximum of χ''
$[Co(H_2bapbh)(H_2O)(NO_3)]\cdot(NO_3)$[41]	0.335 9.84 170.8	+33.1; 0^m +41.1; 0^N	0.4 (@2.0 K,0.2T) 31.1; 3.63×10^{-7} O 48.7; 3.69×10^{-8} OD
$[M(L5)](ClO_4)_2\cdot1.5CH_3NO_2$[42]	1.2/1.2 4.4/3.7 169.6/170.9	+40.3; 0.1^m +34.0; 0.09^N	0.4 (@1.9 K, 0.1T) 6.0; 6.0×10^{-6} O
$[Co\text{-}(DAPBH)(NO_3)(H_2O)](NO_3)$[43]	0.417 12.96 173.59	+31.0; 0^m +35.4; 0.06^N	- (@0.1T) ≈ 50 K
$[Co(tbp)_3(NO_3)_2]$[44,40]	1.41 70.1 171.9	+35.8; 0^m +62; 0.25^N	5.4 (@1.8 K, 0.1T) 17.7; 7.68×10^{-7} O
$[Co(isq)_3(NO_3)_2]$[44,40]	1.54 66.0	+35.7; 0^m +41.4; 0.11^N	- (@0.1T)

	172.6		11.0; 7.01×10^{-7} O
[Co(tmpdt)$(NO_3)_2$]CH_3CN[45,40]	2.217 62.26 166.4	+37.4; 0.31[m] +37.4; 0.18[HFEPR]	4.8 (@1.8 K, 0.1T)
			Orbach process not operative
[Co(L6)$(NO_3)_2(CH_3CN)$][46]	2.050 64.7 177.6	28.3; 0.10[m] 29.7; 0.16[NC]	0.26 (@1.9 K, 0.09T)
			Orbach process not operative
[Co(L7S)$(NO_3)_2(H_2O)$][46]	2.038/1.908 64.4/62.6 173.4/173.4	22.2; 0.06[m] 29.4; 0.16/31.2; 0.16[NC]	1.10 (@1.9 K, 0.125T)
			Orbach process not operative
[Co(L7R)$(NO_3)_2(H_2O)$][46]	1.935/2.029 63.1/64.3 173.4/173.5	25.9; 0.06[m] 0.17; 0.17 [NC]	1.79 (@1.9 K, 0.125T)
			Orbach process not operative
[Co2(L)$(\kappa^2\text{-}NO_3)_2$] compound **3**, this work	2.802 60.5 153.96	+39.3; 0.16[m] +36.77; 0.24[N]	3.55 (@1.9 K, 0.125T)
			27; 1.7×10^{-8} O 31; 5×10^{-9} OD

[m] parameters obtained from fitting of DC magnetic data; [N]calculated parameters, CASSCF+NEVPT2; [iii)] relaxation time τ at the lowest temperature of measurement and given DC field; [O] single Orbach fit from high temperature region of lnτ vs 1/T; [OR] Orbach&Raman fit from high temperature region of lnτ vs 1/T; [OD] Orbach&direct fit from high temperature region of lnτ vs 1/T; **pypzbeyz** = N-((6-(1H-pyrazol-1-yl)pyridin-2-yl)methylene)benzohydrazide); **H_2L1** = 2,2′-[2,6-pyridinediylbis(ethylidyne-1-hydrazinyl-2-ylidene)]bis[N,N,N-trimethyl-2-oxoethanaminium]; **L2** = {3,12-bis(2-methylpyridine)-3,12,18-triaza-6,9-dioxabicyclo[12.3.1]octadeca-1,14,16-triene; **L3**= 3,12,18-triaza-6,9-dioxabicyclo[12.3.1]octadeca-1(18),14,16-triene; **H_2dapb** = 2,6-diacetylpyridine bis(benzoylhydrazine); **L4** = 2,13-dimethyl-3,6,9,12-tetraaza-1(2,6)-pyridine-cyclotridecaphane-2,12-diene; **im** = imidazole; **Hdapbh** = (N',N'"E,N',N'"E)-N',N'"-(pyridine-2,6-diylbis(ethan-1-yl-1-ylidene))di(benzohydrazide); **H_2aapbh** = N',N'"-{pyridine-2,6-diyldi[(1E)-ethan-1-yl-1-ylidene]}diformohydrazide; **H_2bapbh**=N',N"-{pyridine-2,6-diyldi[(1E)-ethan-1-yl-1-ylidene]}diacetohydrazide; **L5** = 3,12-bis((1H-benzimidazol -2-yl)methyl)-6,9-dioxa-3,12,18-triazabicyclo[12.3.1]octadeca-1(18),14,16-triene; **py** = pyridine; **tbp**= 4-tert-butylpyridine; **isq** = isoquinoline; **L6** = 1-pentyl-2-(pyridin-2-yl)-1H-benzimidazole; **L7S** = 1-[(2S)-2-methylbutane-1-yl]-2-(pyridine-2-yl)-1*H*-benzimidazole; **L7R** = 1-[(2R)-2-methylbutane-1-yl]-2-(pyridine-2-yl)-1*H*-benzimidazole.

Table S24 Heptacoordinate Co(II)-SIMs with non-pentagonal bipyramid geometry

	COC-7 CTPR-7 PBPY-7	***D*(cm^{-1}); E/D**	***τ*[iii)] (ms)** ***U*$_{eff}$ (K); τ_0(s)**
[Co(tmpdc)$(NO_3)_2$][45]	3.13 2.44 8.08	+4.7; 0.2[m] |3.65|; 0.18[HFEPR]	0.32 (@1.8 K,0.15T) Orbach process not operative
[(OTftpy)Co(κ_2-$O_2NO)_2$][47]	3.09 2.04 7.40	−41.4; 0.11[m] −7.23; 0.18[N]	not measured
[Co(DQ)(OTf)](OTf)·H_2O[48]	5.05 3.79 4.00	+12.9; 0[m] +18.0; 0.3[N]	2.3 (@1.8 K,0.125T) 21.1; 6.74×10^{-7}
[Co(BPA-TPA)]$(BF_4)_2$[49]	3.28 2.72 4.95	+13.1; 0[m]	0.04 (@1.8 K,0.1T) 39.7; 1.5×10^{-9} O 45.0; 3.1×10^{-10} OD
Co(BPA-TPA)]$(ClO_4)_2$·H_2O[49]	2.97 2.54 5.14	+15.4; 0[m]	0.05 (@1.8 K,0.04T) no maximum of χ''

[Co(BPA-TPA)](PF$_6$)$_2$[49]	2.23/2.59 2.26/3.17 7.00/7.73	+10.0; 0[m]	0.5 (@1.8 K,0.1T) 9.1; 3.7×10^{-6} [O]
[Co(BPA-TPA)](BPh$_4$)$_2$[49]	3.95 3.68 2.75	+14.6; 0[m]	0.7 (@1.8 K,0.06T) 4.8; 5.0×10^{-5} [O]
[Co(napy)$_4$](ClO$_4$)$_2$[50]	5.17 4.03 4.19	+25.3; 0.35[m] +26.7; 0.31[N]	4.8 (@1.8 K,0.1T) 32.0; 3.1×10^{-8} [O] 61.3; 2.6×10^{-9} [OR]
(MePh$_3$P)$_2$[Co(NO$_3$)$_4$] [51]	6.20 5.58 5.29	+23.2; 0.03[m] +19.0; 0.30[N] +12.7; 0.17[HFEPR]	4.9 (@1.8 K,0.06T) 20.0; 2.1×10^{-9} [O] 26.6; 1.9×10^{-11} [OR]
[Co1(L)(κ^2-NO$_3$)$_2$] compound **3**, this work	4.454 2.704 4.537	−10.1; 0.30[m] −17.62; 0.23[N]	3.55 (@1.9 K, 0.125T) 27; 1.7×10^{-8} [O] 31; 5×10^{-9} [OD]

[m] parameters obtained from fitting of DC magnetic data; [N]calculated parameters, CASSCF+NEVPT2; [iii] relaxation time τ at the lowest temperature of measurement and given DC field; [O] single Orbach fit from high temperature region of lnτ vs 1/T; [OR] Orbach&Raman fit from high temperature region of lnτ vs 1/T; [OD] Orbach&direct fit from high temperature region of lnτ vs 1/T; **tmpdc** = N,N,N',N'-tetramethyl-2,6-pyridinedicarboxamide; **tmpdt** = N,N,N',N'-tetramethyl-2,6-pyridine-dithiocarboxamide; **OTftpy** = 4'-trifluoromethylsulfonate-2,2':6',2''-terpyridine; **DQ** = 6,6″-di(quinolin-8-yl)-4′- phenyl-2,2′:6′,2″-terpyridine; **BPA-TPA** =2,6-bis(bis(2-pyridylmethyl)amino)methyl-pyridine; **napy** =1, 8-naphthyridine

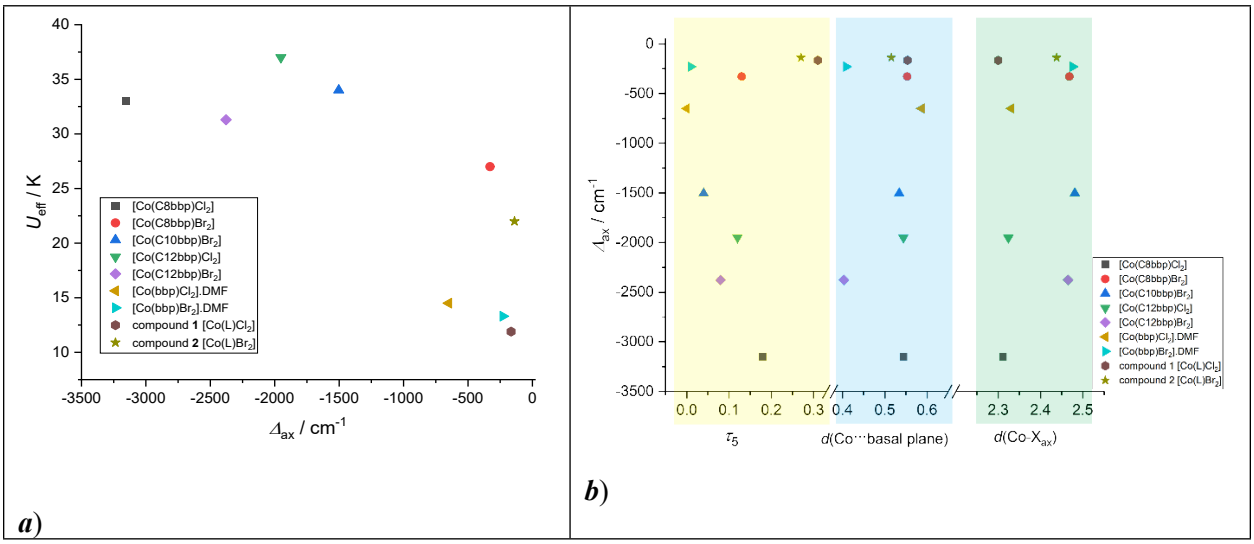

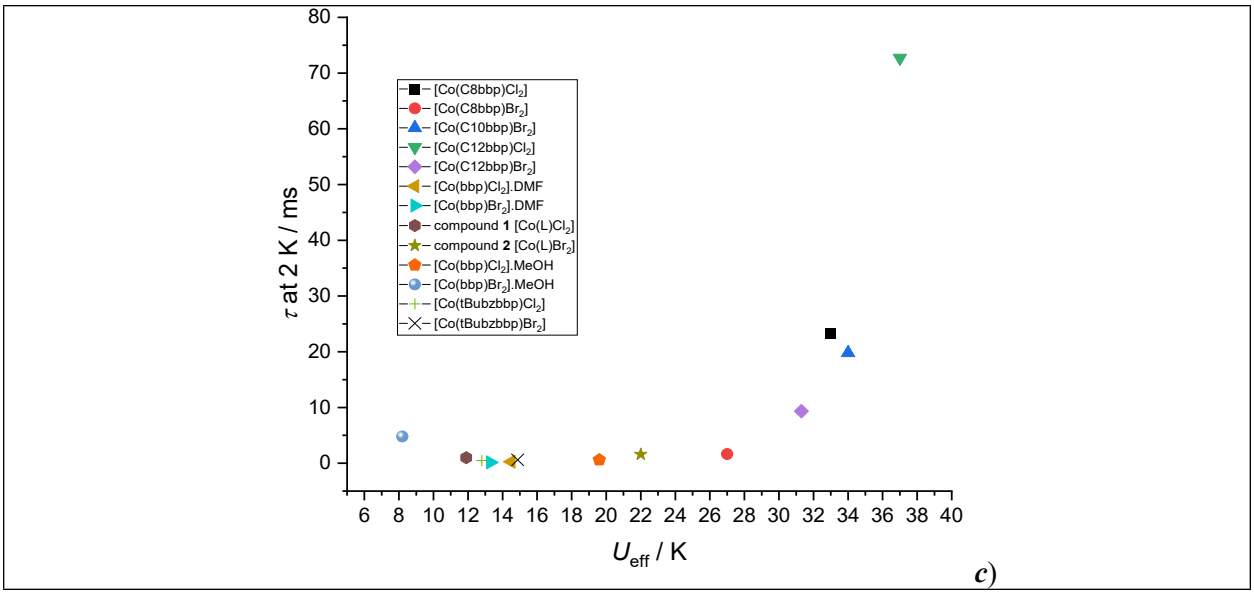

Figure S 26 Evolution of ***a***) U_{eff} vs. Δ_{ax} and ***b***) Δ_{ax} vs. τ_5 (*left*), Δ_{ax} vs. *d*(Co···basal plane) (*middle*) and Δ_{ax} vs. Co-X_{ax} (*left*) in the family of [Co(Rbbp)X_2] (X=Cl, Br) complexes with square-pyramidal geometry of coordination polyhedra. Compounds [Co(tBuBzbbp)X_2] and [Co(bbp)X_2]·MeOH are not involved in the magneto-structural correlations due their trigonal bipyramidal geometry and the absence of GFH parameters, respectively. c) Correlation of relaxation time τ at 2 K with U_{eff} obtained from Arrhenius-type fits of the linear regions of lnτ vs. 1/T

S7 References

[1] A. Addison, P. Burke, *J. Heterocycl. Chem.*, 1981, **18**, 803–805.
[2] Rigaku Oxford Diffraction, *CrysAlisPro*, 2020, 1.171.40.82a.
[3] G. M. Sheldrick, *Acta Crystallogr. Sect. A*, 2015, **71**, 3–8.
[4] L. J. Bourhis, O. V. Dolomanov, R. J. Gildea, J. A. K. Howard, H. Puschmann, *Acta Crystallogr. Sect. A*, 2015, **71**, 59–75.
[5] O. V. Dolomanov, L. J. Bourhis, R. J. Gildea, J. A. K. Howard, H. Puschmann, *J. Appl. Crystallogr.*, 2009, **42**, 339–341.
[6] R. Boča, *Theoretical Foundations of Molecular Magnetism*, Elsevier, Amsterdam, 1999.
[7] (a) F. Neese, *WIREs Comput. Mol. Sci.*, 2025, **15**, e70019; (b) F. Neese, *WIREs Comput. Mol. Sci.*, 2022, **12**, e1606; (c) F. Neese, *WIREs Comput. Mol. Sci.*, 2018, **8** (1), 1327; (d) F. Neese, *WIREs Comput. Mol. Sci.*, 2012, **2** (1), 73–78; (e) F. Neese, *J. Comput. Chem.*, 2023, **44** (3), 381–396; (f) F. Neese, F. Wennmohs, U. Becker, C. Riplinger, *J. Chem. Phys.*, 2020, **152**, 224108.
[8] (a) L. Ungur, M. Thewissen, J.-P. Costes, W. Wernsdorfer, L. F. Chibotaru, *Inorg. Chem.*, 2013, **52** (11), 6328–6337; (b) L. F. Chibotaru, L. Ungur, A. Soncini, *Angew. Chem. Int. Ed.*, 2008, **47**, 4126–4129; (c) L. Ungur, W. Van Den Heuvel, L. F. Chibotaru, *New J. Chem.*, 2009, **33** (6), 1224–1230; (d) L. F. Chibotaru, L. Ungur, C. Aronica, H. Elmoll, G. Pilet, D. Luneau, *J. Am. Chem. Soc.*, 2008, **130** (37), 12445–12455; (e) L. F. Chibotaru, L. Ungur, *J. Chem. Phys.*, 2012, **137** (6), 064112.
[9] (a) R. Izsák, F. Neese, W. Klopper, *J. Chem. Phys.*, 2013, **139**, 094111; (b) R. Izsák, A. Hansen, F. Neese, *Mol. Phys.*, 2012, **110** (19–20), 2413–2417; (c) B. Helmich-Paris, B. de Souza, F. Neese, R. Izsák, *J. Chem. Phys.*, 2021, **155**, 104109; (d) A. K. Dutta, F. Neese, R. Izsák, *Mol. Phys.*, 2019, **116** (11), 1428–1434; (e) F. Neese, F. Wennmohs, A. Hansen, U. Becker, *Chem. Phys.*, 2011, 356(1–3), 98–109; (f) R. Izsák, F. Neese, *J. Chem. Phys.*, 2011, **135** (14), 144105.
[10] (a) P. A. Malmqvist, B. O. Roos, *Chem. Phys. Lett.*, 1989, **155** (2), 189–194; (b) C. Kollmar, K. Sivalingam, B. Helmich-Paris, C. Angeli, F. Neese, *J. Comput. Chem.*, 2019, **40** (14), 1463–1470; (c) M. Ugandi, M. A. Roemelt, *Int. J. Quantum Chem.*, 2023, **123** (5), e27045.
[11] (a) C. Angeli, R. Cimiraglia, J.-P. Malrieu, *Chem. Phys. Lett.*, 2002, **350** (3–4), 297–305; (b) C. Angeli, R. Cimiraglia, S. Evangelisti, T. Leininger, J.-P. Malrieu, *J. Chem. Phys.*, 2001, **114** (23), 10252–10264; (c) C. Angeli, R. Cimiraglia, J.-P. Malrieu, *J. Chem. Phys.*, 2002, **117** (20), 9138–9153.
[12] F. Weigend, R. Ahlrichs, *Phys. Chem. Chem. Phys.*, 2005, **7** (18), 3297–3305.
[13] F. Weigend, *Phys. Chem. Chem. Phys.*, 2006, **8**, 1057–1065.
[14] A. Hellweg, C. Hattig, S. Hofener, W. Klopper, *Theor. Chem. Acc.*, 2007, **117**, 587–597.
[15] (a) L. Lang, F. Neese, *J. Chem. Phys.*, 2019, **150**, 104104; (b) D. Ganyushin, F. Neese, *J. Chem. Phys.*, 2013, **138**, 104113; (c) D. Ganyushin, F. Neese, *J. Chem. Phys.*, 2006, **125**, 24103.
[16] F. Neese, *J. Chem. Phys.*, 2005, **122** (3), 034107.
[17] R. Maurice, R. Bastardis, C. de Graaf, N. Suaud, T. Mallah, N. Guihéry, *J. Chem. Theory Comput.*, 2009, **5** (11), 2977–2984.
[18] (a) C. Lee, W. Yang, R. G. Parr, *Phys. Rev. B*, 1988, **37** (2), 785–789; (b) A. D. Becke, *J. Chem. Phys.*, 1993, **98** (7), 5648–5651; (c) S. H. Vosko, L. Wilk, M. Nusair, *Can. J. Phys.*, 1980, **58** (8), 1200–1211; (d) P. J. Stephens, F. J. Devlin, C. F. Chabalowski, M. J. Frisch, *J. Phys. Chem.*, 1994, **98** (45), 11623–11627.
[19] N. F. Chilton, R. P. Anderson, L. D. Turner, A. Soncini, K. S. Murray, *J. Comput. Chem.*, 2013, **34** (13), 1164–1175.
[20] A. D. Becke, *Phys. Rev. A*, 1988, **38** (6), 3098–3100.
[21] (a) D. Peng, N. Middendorf, F. Weigend, M. Reiher, *J. Chem. Phys.*, 2013, **138**, 184105; (b) Y. J. Franzke, N. Middendorf, F. Weigend, *J. Chem. Phys.*, 2018, **148**, 104110; (c) L. Cheng, J. Gauss, *J. Chem. Phys.*, 2011, **135**, 084114.
[22](a) P. Pollak, F. Weigend, *J. Chem. Theory Comput.*, 2017, **13** (8), 3696–3705; (b) Y. J. Franzke, R. Treß, T. M. Pazdera, F. Weigend, *Phys. Chem. Chem. Phys.*, 2019, **21** (30), 16658–16664.
[23] G. L. Stoychev, A. A. Auer, F. Neese, *J. Chem. Theory Comput.*, 2017, **13** (2), 554–562.
[24] E. R. Sayfutyarova, Q. Sun, G. K. L. Chan, G. Knizia, *J. Chem. Theory Comput.*, 2017, **13** (9), 4063–4078.
[25] (a) M. Atanasov, D. Ganyushin, K. Sivalingam, F. Neese, *Structure and Bonding*, 2011, 149–220; (b) L. Lang, M. Atanasov, F. Neese, *J. Phys. Chem. A*, 2020, **124** (5), 1025–1037; (c) D. Aravena, M. Atanasov, F. Neese, *Inorg. Chem.*, 2016, **55** (9), 4457–4469;

(d) J. Jung, M. Atanasov, F. Neese, *Inorg. Chem.*, 2017, **56** (15), 8802–8816.
[26] M. D. Hanwell, D. E. Curtis, D. C. Lonie, T. Vandermeersch, E. Zurek, G. R. Hutchison, *J. Cheminform.*, 2012, **4** (1), 17.
[27] K. Momma, F. Izumi, *J. Appl. Crystallogr.*, 2011, **44** (6), 1272–1276.
[28] C. F. Macrae, P. R. Edgington, P. McCabe, E. Pidcock, G. P. Shields, R. Taylor, M. Towler, J. van de Streek, *J. Appl. Crystallogr.*, 2006, **39** (3), 453–457.
[29] J. Juráková, J. D. M. Midlíková, J. Hrubý, A. Kliuikov, V. T. Santana, J. Pavlik, J. Moncoľ, E. Čižmár, M. Orlita, I. Mohelský, P. Neugebauer, D. Gentili, M. Cavallini, I. Šalitroš, *Inorg. Chem. Front.*, 2022, **9**, 1179–1194.
[30] N. Malinová, J. Juráková, B. Brachňaková, J. Dubnická Midlíková, E. Čižmár, V. T. Santana, R. Herchel, M. Orlita, I. Mohelský, J. Moncoľ, P. Neugebauer, I. Šalitroš, *Cryst. Growth Des.*, 2023, **23**, 2430.
[31] A. K. Mondal, T. Goswami, A. Misra, S. Konar, *Inorg. Chem.*, 2017, **56**, 6870.
[32] C. Rajnák, F. Varga, J. Titiš, J. Moncoľ, R. Boča, *Eur. J. Inorg. Chem.*, 2017, **13**, 1915.
[33] B. Brachňaková, S. Matejová, J. Moncoľ, R. Herchel, J. Pavlik, E. Moreno-Pineda, M. Ruben, I. Šalitroš, *Dalton Trans.*, 2020, **49**, 1249–1264.
[34] X.-C. Huang, W. Yong, S. Moorthy, Z.-Y. Su, J.-J. Kong, S. K. Singh, *Polyhedron*, 2023, **232**, 116275.
[35] D. Darmanović, I. N. Shcherbakov, C. Duboc, V. Spasojević, D. Hanžel, K. Anđelković, D. Radanović, I. Turel, M. Milenković, M. Gruden, B. Čobeljić, M. Zlatar, *J. Phys. Chem. C*, 2019, **123**, 31142–31155.
[36] A. K. Mondal, A. Mondal, B. Dey, S. Konar, *Inorg. Chem.*, 2018, **57**, 9999–10008.
[37] P. Antal, B. Drahoš, R. Herchel, Z. Trávníček, *Inorg. Chem.*, 2016, **55**, 5957–5972.
[38]B. Drahoš, R. Herchel, Z. Trávníček, *Inorg. Chem.*, 2015, **54**, 3352–3369.
[39] X.-C. Huang, C. Zhou, D. Shao, X.-Y. Wang, *Inorg. Chem.*, 2014, **53**, 12671–12673.
[40] P. Comba, G. Rajaraman, A. Sarkar, G. Velmurugan, *Dalton Trans.*, 2022, **51**, 5175–5183.
[41] Y. Qin, Y. Wu, S. Luo, J. Xi, Y. Guo, Y. Ding, J. Zhang, X. Liu, *Dalton Trans.*, 2022, **51**, 17089–17096.
[42] B. Drahoš, I. Císařová, O. Laguta, V. T. Santana, P. Neugebauer, R. Herchel, *Dalton Trans.*, 2020, **49**, 4425–4440.
[43] (a) F. Habib, I. Korobkov, M. Murugesu, *Dalton Trans.*, 2015, **44**, 6368–6373; (b) R. Ruamps, L. J. Batchelor, R. Maurice, N. Gogoi, P. Jimenez-Lozano, N. Guihéry, C. de Graaf, A.-L. Barra, J.-P. Sutter, T. Mallah, *Chem. Eur. J.*, 2013, **19**, 950–956.
[44] S.-Y. Chen, Y.-C. Sun, Y.-M. Guo, L. Yu, X.-T. Chen, Z. Wang, Z. W. Ouyang, Y. Song, Z.-L. Xue, *Dalton Trans.*, 2015, **44**, 11482–11490.
[45] W. Lv, L. Chen, X.-T. Chen, H. Yan, Z. Wang, Z.-W. Ouyang, Z.-L. Xue, *New J. Chem.*, 2023, **47**, 15553–15560.
[46] A. Šagátová, I. Nemec, J. Moncoľ, R. Herchel, R. Šebesta, P. Kisszékelyi, L. Ďurina, I. Šalitroš, *Inorg. Chem. Front.*, 2025, accepted, DOI: 10.1039/d5qi01269d.
[47] R. F. Higgins, B. N. Livesay, T. J. Ozumerzifon, J. P. Joyce, A. K. Rappé, M. P. Shores, *Polyhedron*, 2018, **143**, 193–200.
[48] M.-M. Zeng, Z.-Y. Ruan, W. Deng, S.-G. Wu, M.-L. Tong, *Inorg. Chem. Commun.*, 2024, **165**, 112551.
[49] (a) G. Yi, C. Zhang, W. Zhao, H. Cui, L. Chen, Z. Wang, X.-T. Chen, A. Yuan, Y.-Z. Liu, Z.-W. Ouyang, *Dalton Trans.*, 2020, **49**, 7620–7627; (b) G. Yi, H. Cui, C. Zhang, W. Zhao, L. Chen, Y.-Q. Zhang, X.-T. Chen, Y. Song, A. Yuan, *Dalton Trans.*, 2020, **49**, 2063–2067.
[50] X.-C. Huang, R. Xu, Y.-Z. Chen, Y.-Q. Zhang, D. Shao, *Chem. Asian J.*, 2020, **15**, 279–286.
[51] L. Chen, H.-H. Cui, S. E. Stavretis, S. C. Hunter, Y.-Q. Zhang, X.-T. Chen, Y.-C. Sun, Z. Wang, Y. Song, A. A. Podlesnyak, Z.-W. Ouyang, Z.-L. Xue, *Inorg. Chem.*, 2016, **55**, 12603–12617.